2020

Relating Sonic Velocities, Minimum Horizontal Stress, and Natural Fracture Distribution to Stimulation Efficiency during Completion of the Marcellus Shale MIP-3H Unconventional Well, West Virginia, USA

Kaitlin Gayle Evans
kge0002@mix.wvu.edu

Relating Sonic Velocities, Minimum Horizontal Stress, and Natural Fracture Distribution to Stimulation Efficiency during Completion of the Marcellus Shale MIP-3H Unconventional Well, West Virginia, USA

Kaitlin G. Evans

Thesis submitted to the
Eberly College of Arts and Sciences
at West Virginia University

in partial fulfillment of the requirements for the degree of

Master of Science in
Geology

Timothy R. Carr, Ph.D., Chair
Jaime Toro, Ph.D.
Payam Kavousi, Ph.D.

Department of Geology and Geography

Morgantown, West Virginia
2020

Key Words: Marcellus Shale, Geomechanics, Distributed Acoustic Sensing, Fracture Distribution

ABSTRACT

Relating Sonic Velocities, Minimum Horizontal Stress, and Natural Fracture Distribution to Stimulation Efficiency during Completion of the Marcellus Shale MIP-3H Unconventional Well, West Virginia, USA

Kaitlin G. Evans

Log data from the Marcellus Shale Energy and Environment Laboratory (MSEEL) was acquired along the lateral of the MIP-3H well. This unconventional shale-gas well was completed within the Marcellus Shale just above the Cherry Valley Limestone, a thin limestone member separating organic rich units of the Marcellus. The geomechanical moduli, Poisson's Ratio (PR) and Young's Modulus (YME), were generated using compressional and shear sonic logs to indicate zones of increasing brittleness for each of the 28 stages along the 6124 ft. (1867m) horizontal lateral. Brittle reservoir rock is more readily fractured during hydraulic stimulation than more malleable rock. Stages with geomechanically homogeneous clusters were more likely to have evenly distributed energy during stimulation. Natural fractures formed during maturation of the Marcellus Shale are interpreted to have initiated during the Permian and are distributed along the wellbore. The contrast between calcite and shale in Schlumberger Quanta Geo logs facilitated fracture identification, and 1600 calcite-filled and a few open pre-existing fractures were recognized along the horizontal portion of the well. Research conducted suggests that all pre-existing fractures are reactivated during hydraulic stimulation and contribute to the complex fracture network. Because these fractures are reactivated during the hydraulic fracturing process, natural fracture intensity and distribution within stages can impact the efficiency of stimulation. Minimum horizontal stress (Sh_{min}) is an important factor to consider in the completion process. Cluster placement at locations of equal or similar Sh_{min} allows for fracturing fluid to more evenly disperse across all perforations. Hydraulic stimulation data were obtained with the use of a fiber optic cable. The distributed acoustic sensing (DAS) data allows for a comparison of the energy distribution during stimulation. Comparing geomechanical properties of individual stages to the apparent stimulation efficiency shown in the DAS data can result in improved methods of well completion. This would lead to more geologic approaches to stage and perforation completion rather than geometric. Increased stimulation efficiency could increase production and estimated ultimate recovery from unconventional shale-gas reservoirs.

Table of Contents

Figures in Text

Tables in Text

1. Introduction

Unconventional shale reservoirs are a major producer of natural gas and in 2018 represented 69% of total U.S. dry natural gas production (EIA, 2019). Unconventional shale hydrocarbon systems have resulted in an abundant natural gas energy supply, and with continued research and exploration efforts, production efficiency from these reservoirs will continue to improve. Natural gas production, primarily from shale gas, is forecasted to continue to increase through 2050 (EIA, 2020). Efforts to improve production efficiency are important as it is estimated that only about 25% of dry gas is recovered from unconventional shale gas wells (Zoback and Kohli, 2019). Creation of artificial permeability in horizontal wells through an induced fracture network is critical to the development of shale-gas reservoirs. Because of this, efficient fracturing of completion stages is an important factor for economic production of the source rock.

Unconventional shale reservoirs are unique in that they are the source rock, reservoir rock, and trap for the petroleum system, and factors resulting in improved economic production of these reservoirs have remained somewhat of a mystery and are termed a statistical play. King (2014) indicates that economic production from shale wells varies significantly with one third uneconomic, one third only economic when gas prices are high, and one third producing so well they make up for the lack of production in the previous two thirds with no real explanation as to why. Traditional reservoir evaluation and conventional production methods have proven to be inadequate; simply perforating and pumping massive hydraulic fracture treatments into formations containing natural gas is often inefficient and does not consistently yield economical results (Grieser and Bray, 2007). Targeted horizontal drilling of gas-rich zones in core areas and geologic “sweet spots” is only one component of extracting natural gas from shale reservoirs and does not completely mitigate the statistical nature of shale gas. Research into other factors such

as pre-existing fractures and faults or reservoir pore pressure potentially contributing to completion and production efficiency is essential for effective development of unconventional shale resources.

Analyzing the varying geomechanical properties of individual hydraulic fracturing stages within an unconventional shale well is one method of increasing the efficiency of natural gas extraction. Geomechanical properties, such as rigidity and brittleness, are useful when identifying reservoirs more susceptible to fracture stimulation and can contribute to a better understanding of the relationship of "fracability" to completion efficiency and the subsequent production. Observing stage stimulation efficiency may lead to overall improvement in well production. The goal of this research is to better understand the geomechanical properties resulting in more effective completion techniques for unconventional shale-gas wells that contribute to improved hydraulic fracturing stimulation and subsequent natural gas production.

1.1 Marcellus Shale Background

The Marcellus Shale is a Devonian formation located within the Appalachian basin. The prospective area of the Marcellus covers over 114,000 square kilometers and includes Pennsylvania, West Virginia, Maryland, New York, and Ohio (Zagorski et al., 2017). The Acadian orogeny resulted in basin subsidence during the Middle Devonian and formed the Acadian foreland basin west of the Acadian mountains and east of the Cincinnati arch. At this time, eustatic sea-level rise caused a transition in Early Devonian deposition from sandstone and carbonate to the organic-rich mud that formed the Marcellus Shale and other Devonian shale units. At the time of deposition, the paleoclimate was thought to be warm with seasonally restricted rainfall and occasional large storms (Woodrow and Sevon, 1985; Werne et al., 2002).

Figure 1 Reconstruction of Middle Devonian paleogeography (from Blakey, 2010). The location of the study well (MIP-3H) is representing by the orange dot in the middle of the basin.

The Marcellus Shale is the depositional result of restricted circulation and accumulation of organic matter, and deposition of this formation occurred over a period of 2 million years (Wang and Carr, 2013). This resulted in a mudstone system with high organic content and thin interbedded limestone. The Marcellus has 2.0-13.0 weight percent (wt. %) total organic carbon (TOC), 35 wt. % silica, and 25 wt.% carbonate content (Jarvie, 2012). The stratigraphy surrounding the Marcellus Shale is shown in **figure 2a**. The Marcellus is bounded below by the Onondaga Limestone and is overlain by the Mahantango Formation. Most of the overlying Mahantango Formation is a siltstone or mudstone, but the organic content is significantly lower than the Marcellus, which reflects a fundamental change in the depositional environment. The

Cherry Valley Limestone is one of the thin limestone stringers that separates organic-rich units in the Marcellus. The MIP-3H well was drilled horizontally above the Cherry Valley, and the contrast between the organic-rich shale and the limestone was used to geosteer and keep within the target zone in the Marcellus. Evaluation of geosteering logs indicate that the lateral wellbore was within the targeted horizon more than 95% of lateral length. The location of the MIP-3H within the stratigraphy and in relation to the target zone is shown in **figure 2b**.

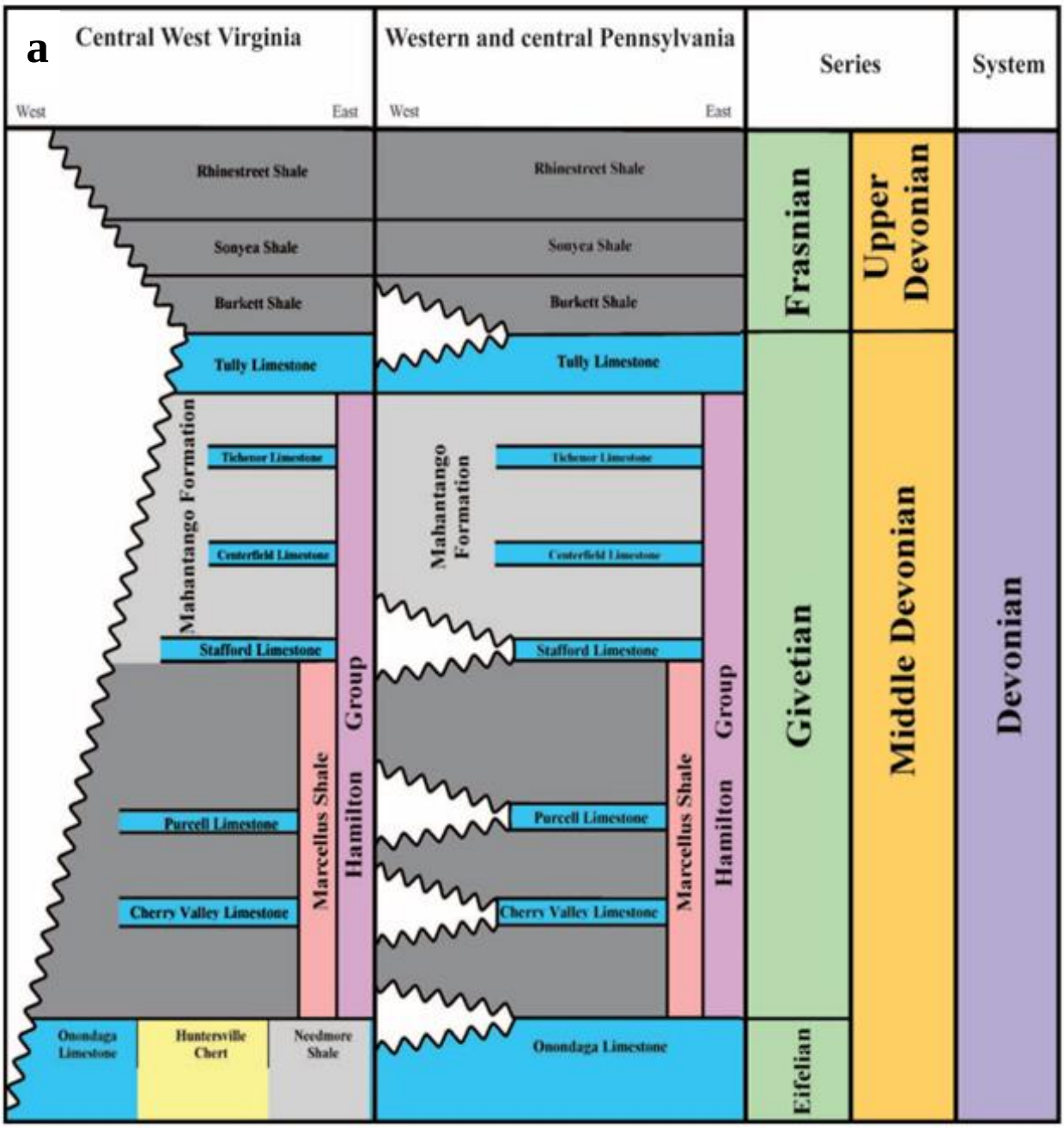
a
Central West Virginia
West
East
Western and central Pennsylvania
West
East
Series
System
Rhinestreet Shale
Sonyea Shale
Burkett Shale
Tully Limestone
Mahantango Formation
Tichenor Limestone
Centerfield Limestone
Stafford Limestone
Hamilton Group
Marcellus Shale
Purcell Limestone
Cherry Valley Limestone
Onondaga Limestone
Huntersville Chert
Needmore Shale
Frasnian
Givetian
Eifelian
Upper Devonian
Middle Devonian
Devonian

b

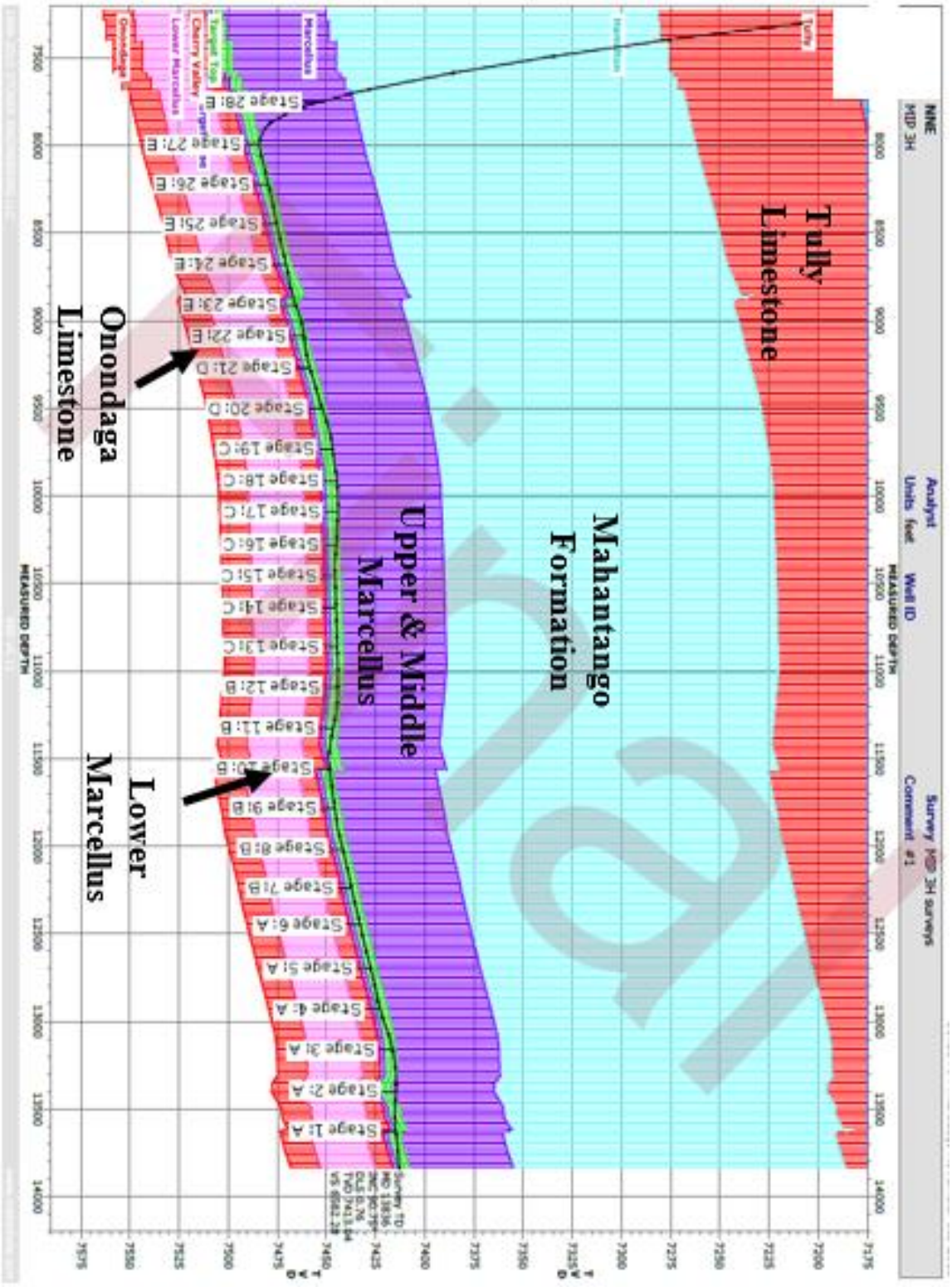

Figure 2 a: Middle Devonian stratigraphy in West Virginia and Pennsylvania (from Zagorski et al., 2012). b: The MIP-3H was kept in the target zone (green) above the Cherry Valley Limestone at the top of the lower Marcellus Shale.

In northern West Virginia and southwestern Pennsylvania, the Marcellus is identified in vertical logs by three intervals of increased gamma ray reading greater than 300 API. In West Virginia, these are separated by two thin limestone beds of lower gamma-ray readings; the Cherry Valley Limestone is the lower bed. X-ray diffraction (XRD) results from Song et al., (2017) demonstrate that organic matter increases as clay content decreases with depth. This XRD data was used to infer the redox potential of the depositional environment during deposition of the Marcellus. The redox conditions of the upper Marcellus are dysoxic while the middle to lower Marcellus range from anoxic to slightly euxinic with an overall reducing environment indicated (Song et al., 2017). **Figure 3** shows a map view of the MIP-3H along with the MIP-4H, MIP-5H, MIP-6H, and observation well of MSEEL, MIP-SW. These wells are located southwest of Morgantown, WV in northern West Virginia. Erosion of Carboniferous and Permian strata accounts for the lack of correlation between thermal index values and the current overburden thickness. Overburden thickness is considered the primary factor for thermal maturation of the Appalachian basin though fluid flow likely also had an impact. Devonian shales in West Virginia typically have high thermal maturity, and these high levels of thermal maturation result in the generation of dry gas. Conodont color alteration index (CAImax) and vitrinite reflectance [%Ro(mean)] values indicate that the Marcellus has reached the dry gas "window" (Repetski et al., 2008) which is supported by the dry gas produced from the well. The Marcellus is one of the most active shale-gas plays in the world, and identifying the factors contributing to economic production is key.

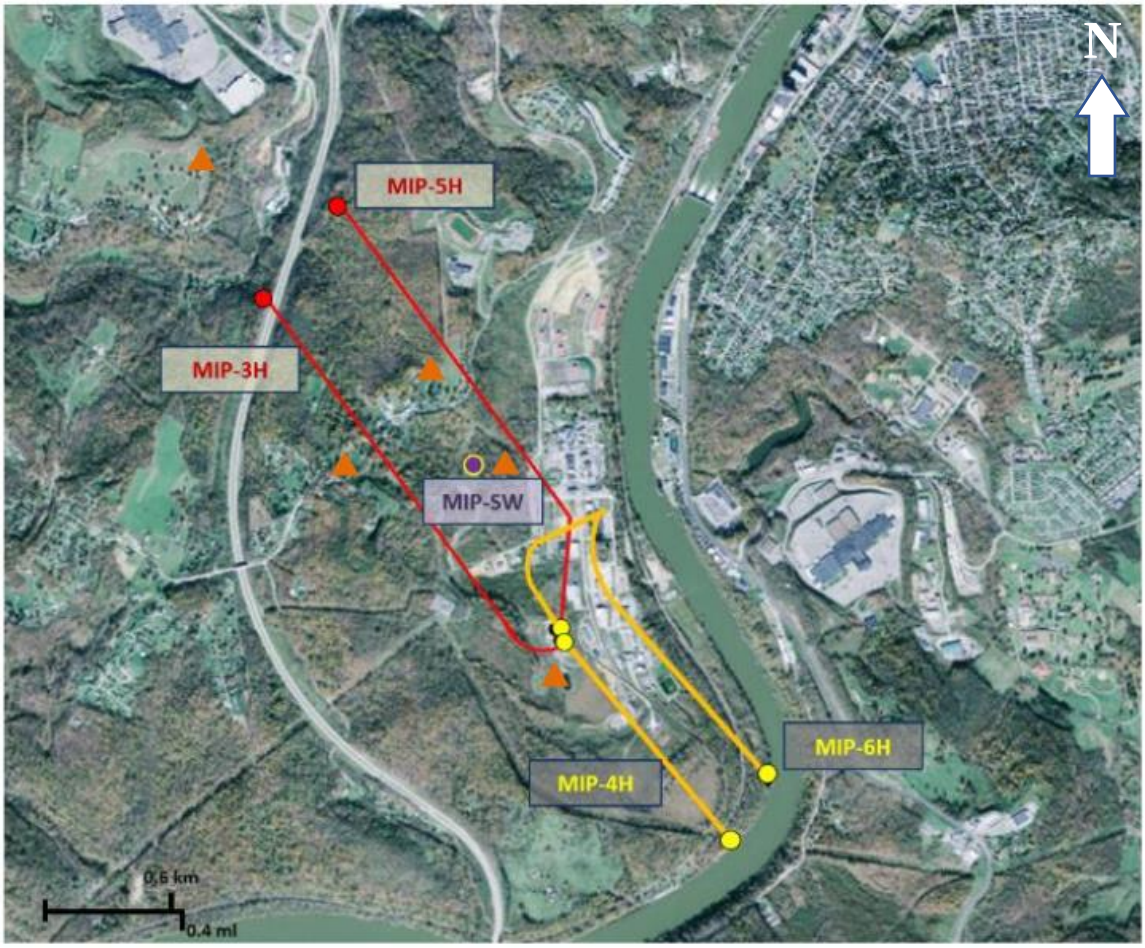

Figure 3: The MSEEL site consists of four horizontal production wells operated by Northeast Natural Energy LLC. (MIP-3H, MIP-4H, MIP-5H, MIP-6H), two pilot holes (MIP-3 and MIP-4), a microseismic observation well (MIP-SW), and a grid of five surface seismometers (triangles).

1.2 MIP-3H Completion

The Marcellus Shale is an example of a shale-gas system that requires induced fracturing of horizontal wells to economically produce hydrocarbons. The horizontal portion of MIP-3H well, located southwest of Morgantown, WV, was drilled in the lower portion of the Marcellus Shale. This well is part of the Marcellus Shale Energy and Environment Laboratory (MSEEL) that works in collaboration with the operator, Northeast Natural Energy LLC., the National Energy Technology Laboratory of the US Department of Energy, as well as several other partners including West Virginia University (Carr et al., 2017).

The MIP-3H is a horizontal, multi-stage well completed from toe to heel as a plugged and perforated well. Completion included twenty-eight stages which were separated into five groups. Stages one through twelve were geometrically spaced. Enhanced engineered completion design was implemented for stages 13-19. Various geomechanical data acquired from well logs were used to optimize the stage length, cluster spacing and treatment parameters. Stages were strategically placed in segments with similar gamma ray, minimum horizontal stress, and natural fracture intensity (Anifowoshe et al., 2016). A limited entry approach was undertaken by decreasing the number of shots per clusters to enhance stimulation efficiency (Anifowoshe et al., 2016). This approach determined stage length, cluster spacing, and treatment (Carr et al., 2017).

Fiber-optic distributed acoustic sensing data and production logging from distributed temperature sensing was used to determine the intensity and efficiency of stimulation as well as estimate the natural gas production from individual completion stages within this well. Fiber optics showed significant variation in energy distribution from stage to stage and that potential production from the individual stages ranged from less than one percent to greater than seven percent.

2. Material and Methodology

Data applied in this analysis was provided by the Marcellus Shale Energy and Environment Laboratory (MSEEL) and their assisting corporations, including operator Northeast Natural Energy. The data was used to implement multiple methods of identifying and evaluating factors contributing to varying efficiency of stage stimulation. This analysis of geomechanical properties isolates factors that resulted in more successful hydraulic stimulation of completion stages in the MIP-3H Marcellus Shale well. The geomechanics that contribute to either high or low stimulation efficiency are found by comparing data obtained and analyzed to the fiber-optic distributed acoustic sensing (DAS) data.

Several logs recorded along the horizontal portion of the well include compressional sonic (DTCO), shear sonic (DTSM), gamma ray, and bulk density (RHOB). Logs of Poisson's Ratio (PR), Young's Modulus (YME), and minimum horizontal stress (Sh_{min}) generate data along the lateral. Schlumberger's Quanta Geo image log was used to identify pre-existing, natural fracture distribution, type, and orientation. Natural fractures were imaged for each stage and identified independently by Keith MacPhail of Schlumberger. Distributed Acoustic Sensing (DAS) fiber optic data were collected and used to evaluate well response to stimulation of individual stages.

2.1 Minimum Horizontal Stress

Research on the Marcellus Shale comparing geometrically completed unconventional shale-gas wells to wells completed using an engineered design was conducted by Walker et al., 2012. Six total wells were included in this analysis: three with geometrical design and three engineered. When determining perforation cluster placement, the engineered design considered the Sh_{min} along the well bore with the goal of causing uniform breakdown of the clusters during stimulation. Clusters were placed in areas of similar stress, and in areas where clusters were at higher stress, the number of perforations was increased to facilitate breakdown of the cluster. The result was an average increase of 100% in the production per foot for the stimulated lateral and an increase of 30% in the estimated ultimate recovery (EUR) (Walker et al., 2012). In this analysis, the average Sh_{min} of the reservoir at each cluster was calculated. The Sh_{min} values for clusters within completion stages was compared to the energy distribution in the DAS data to determine how Sh_{min} magnitude impacts the stimulation of individual stages. The data was viewed as a log, and a method of observing Sh_{min} changes in a reservoir is represented by **equation 1**.

Eq. 1

$$\text{Shmin} = \frac{PR}{1 - PR} * (\sigma - \alpha Pp)$$

Minimum horizontal stress is measured in pounds per square inch (psi) and is calculated using Poisson's Ratio (PR), vertical stress (σ), Biot's Coefficient (α) , and pore pressure (Pp).

Poisson's Ratio is a measurement of the brittleness of reservoir and is discussed later in the paper. Biot's Coefficient is a measurement of the change in fluid volume within a rock in relation to the total change in volume and describes the relative effect of pore pressure on effective stress (Zoback and Kohli, 2019). In general, Biot's Coefficient decreases with increasing simple effective stress (for a given pore pressure) and increases with increasing pore pressure (for a given simple effective stress).

2.2 Poisson's Ratio and Young's Modulus

2.2.1 Shear and Compressional Velocities

Shear and compressional sonic logs, DTSM and DTCO, are used to calculate the shear and compressional sonic velocities incorporated into the geomechanical moduli equations. The shear and compressional velocities are calculated by taking the inverse of the shear and compressional sonic logs in travel time (μS). Shear velocity (Vs) is generated from the shear sonic log, and compressional velocity (Vp) is generated from the compressional sonic log.

Vs is derived from the shear sonic log and is represented by **equation 2**:

Eq. 2

$$\boldsymbol{Vs = \frac{1}{DTSM}}$$

Vp is derived from the compressional sonic log and is represented by **equation 3**:

Eq. 3

$$\boldsymbol{Vp = \frac{1}{DTCO}}$$

The shear and compressional velocities are integrated into the calculations used to generate geomechanical moduli for the Marcellus Shale reservoir in the MIP-3H lateral.

2.2.2 Geomechanical Moduli Generation and Application

Poisson's Ratio (PR) is used to determine the brittleness of a material by measuring the amount of axial compressibility relative to lateral expansion before fracturing occurs. PR is calculated from the amount of lateral expansion of the material when undergoing an axial strain. The division of the lateral expansion by the measured axial shortening gives the Poisson's Ratio value (Zoback, 2007). The less lateral strain relative to axial strain results in a smaller PR value indicating a more brittle material.

Young's Modulus (YME) calculates the rigidity of the reservoir from the elastic deformation of the rock. An ideal elastic material will have a linear relation between the stress applied to the material and the strain experienced. The "stiffness" of the rock, or the resistance to failure, is represented by the Young's Modulus value. Rock will deform elastically except for a small amount of inelastic deformation just before failure. Young's Modulus evaluates the strength of the material by calculating the ratio of stress to strain. A material that experiences less strain as stress is applied yields a larger YME which indicates a more rigid material. YME and PR can be

calculated as static or dynamic values. Static is found from experiments in a laboratory, while dynamic is found from seismic velocity measurements or from compressional and shear sonic logs. Dynamic values tend to be higher than static, but dynamic can be converted to static by calculating the trend from static, laboratory values. Dynamic logs are then adjusted based on the trend found. YME and PR were calculated using sonic log measurements along the MIP-3H wellbore. Those dynamic logs were converted to the static logs used in this analysis (Zoback, 2007). This allowed for the application of Greiser and Bray (2007) PR vs. YME cross-plots.

Poisson's Ratio (PR) and Young's Modulus (YME) calculations are generated from the compressional and shear velocities, Vp and Vs, along with bulk density (ρ). The moduli are represented by equations 3 and 4 shown below.

Eq. 4

Poisson's Ratio: $$PR = \frac{Vp^2 - 2Vs^2}{2\,(Vp^2 - Vs^2)}$$

Eq. 5

Young's Modulus: $$YME = \frac{\rho Vs^2 (3Vp^2 - 4Vs^2)}{Vp^2 - Vs^2}$$

Poisson's Ratio is a unit-less calculation and has values between 0.1 and 0.5 for various geologic materials. Young's Modulus has units of mega-pound per square inch (Mpsi). Mpsi converts to gigapascals (GPa) by multiplying one Mpsi by 6.895 to obtain Young's Modulus values in units of GPa. In the cross-plots used in this study, YME has either a range from 1.0 to 10.0 Mpsi or 1.0 to 15.0 Mpsi. **Figure 4** shows the zone of increased brittleness of rock in a Poisson's Ratio vs. Young's Modulus cross-plot indicated by Greiser and Bray, 2007.

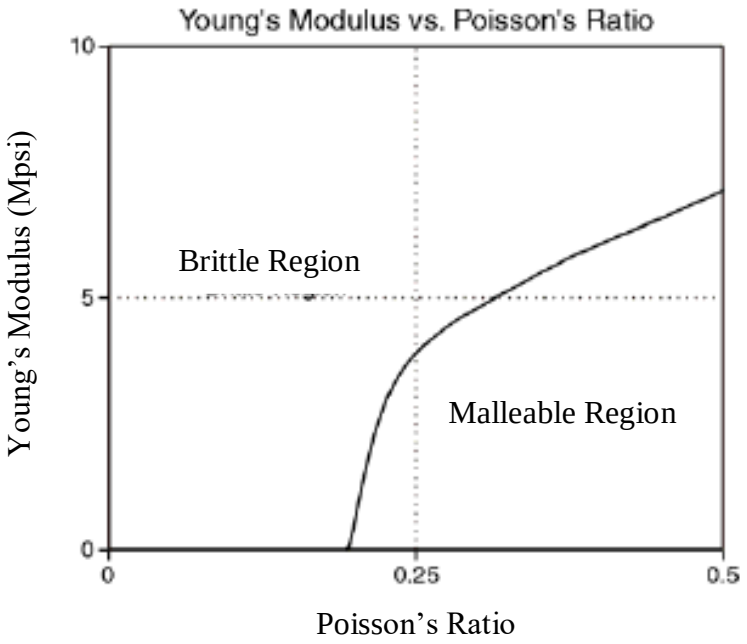

Figure 4 Adapted from (Grieser and Bray, 2007). Displays the general brittle and malleable zones of the Poisson's Ratio vs. Young's Modulus cross-plot.

Greiser and Bray, 2007 suggest that brittle shale will fracture more readily than a malleable shale and will create a larger induced fracture network. A more complex fracture network increases the exposed surface area and increases production. The potential "fracability" of the reservoir can be estimated by analyzing brittleness and rigidity. The average values of Poisson's Ratio and Young's Modulus at each cluster within each stage were compared to the energy distribution across the completion stages during stimulation.

2.2.3 Poisson's Ratio vs. Young's Modulus Cross-Plot

Various lithologies from formations stratigraphically above and below the Marcellus Shale are included in the Young's Modulus (YME) and Poisson's Ratio (PR) cross-plot in **figure 5a**. This cross-plot is used to estimate the brittleness and rigidity of rock represented by the YME and PR values and can also be used to interpret lithology based on the location of data points in the cross-plot. Limestone, like the Tully and Onondaga above and below the Marcellus Shale, are relatively strong with low brittleness and are interpreted to act as barriers to fracture stimulation.

Silica-rich rocks, such as the Huntersville Chert, are relatively rigid and brittle. It is observed where the Onondaga Limestone no longer separates the Marcellus Shale from the Huntersville Chert that fracture stimulation will propagate downward (Zhu, 2019). The data points representing the Mahantango and Marcellus units show that shale can have a large range of geomechanical values. The Marcellus reservoir is relatively brittle when compared with the Mahantango Formation. This brittleness, along with the presence of frac-barriers, make the reservoir susceptible to induced fracturing during hydraulic stimulation. **Figure 5b** shows a very similar placement of data points from the formations discussed above plotted in the cross-plot of minimum horizontal stress (Sh_{min}) and YME. The relationship between Poisson's Ratio and minimum horizontal stress will be discussed later in the results and discussion section of this study.

a

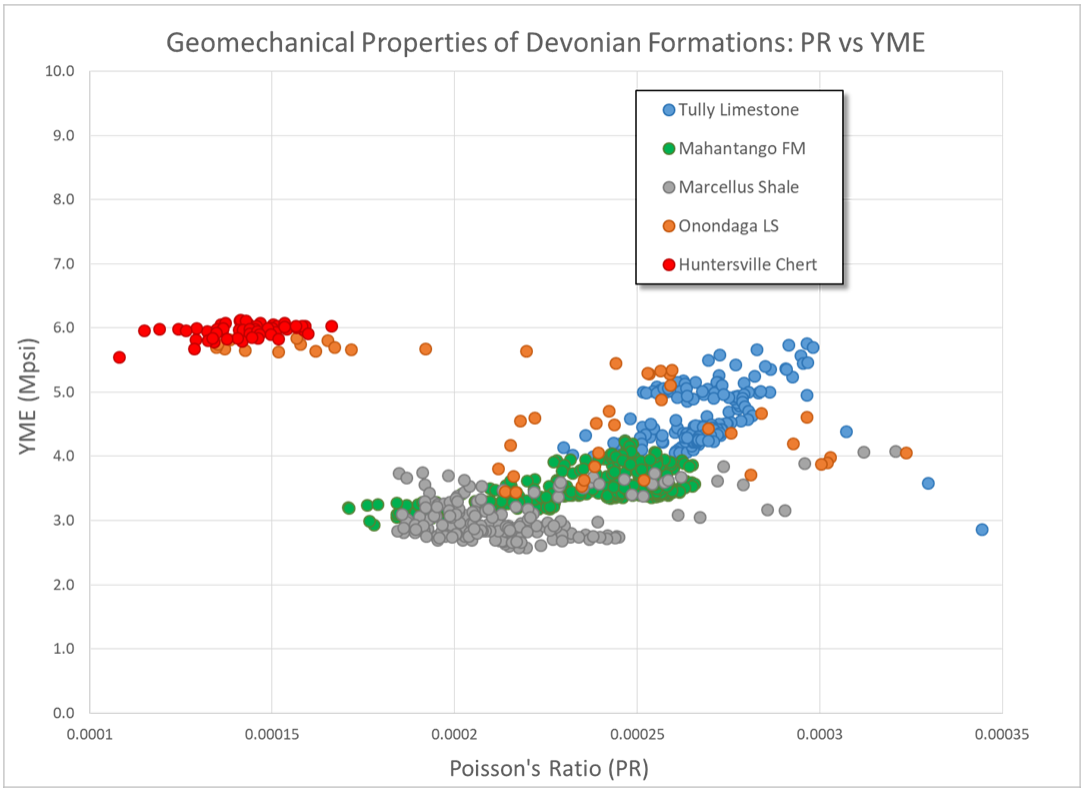

b

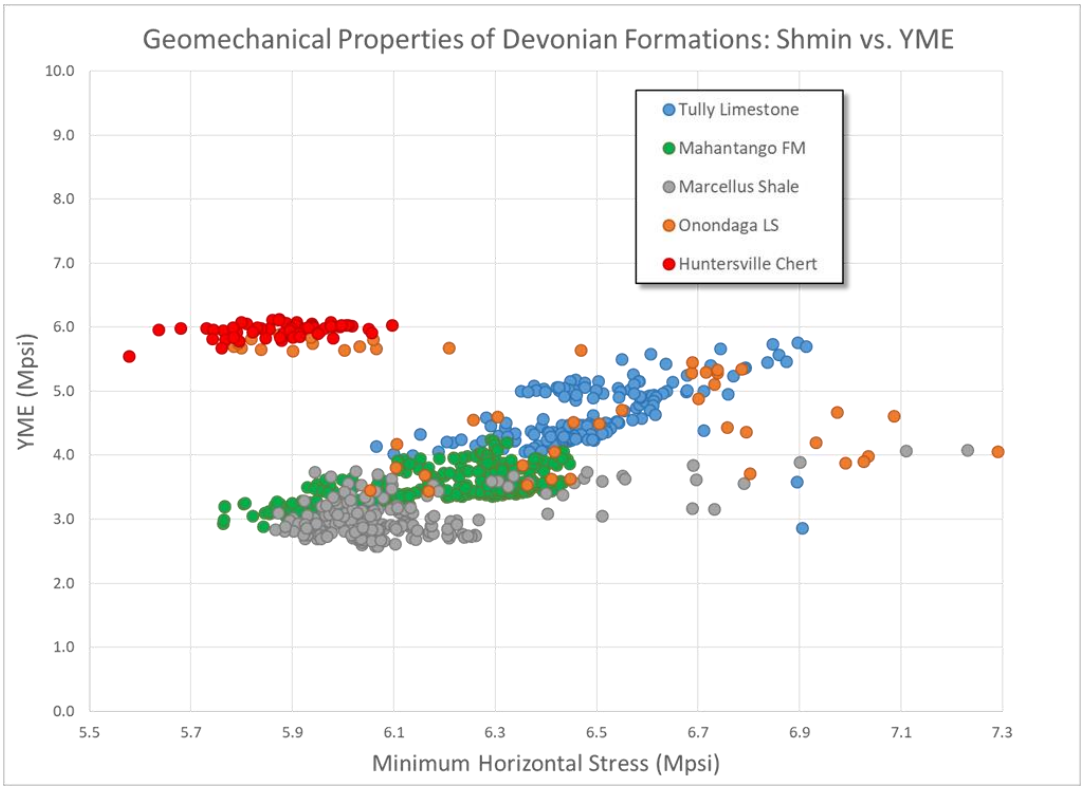

Figure 5 Geomechanical cross-plots of Devonian age formations. 5a. Poisson's Ratio vs. Young's Modulus cross-plot is used to estimate the brittleness and relative strength of various lithologies. 5b. Minimum Horizontal Stress vs. Young's Modulus creates a similar scatter of data points.

2.2.4 Divisions of Standard Deviation using Gamma Ray Log

The standard deviation of Poisson's Ratio (PR) and Young's Modulus (YME) in relation to the gamma ray log was calculated to interpret the heterogeneity within the reservoir. Standard deviation is used to calculate the amount of variation or dispersion of a set of values. The larger the standard deviation, the broader the range around the mean, or average, the values have. For this method of analysis, divisions in the reservoir were created based on the gamma ray log before the standard deviation was calculated for those divisions. This was to locate homogenous zones within the reservoir.

Unconventional shale-gas reservoirs are heterogeneous bodies of rock, so determining geomechanically homogeneous zones prior to fracture stimulation is important. The Marcellus Shale includes numerous natural, calcite-filled fractures, calcite concretions, and laminations and layers within the shale that contribute to the heterogeneity of the reservoir. An approach to quantitatively analyze the reservoir is by examining the deviation of the values within individual stages. Analyzing the standard deviation of geomechanical moduli values is used to evaluate the degree of homogeneity of each stage. The goal of this method was to include the gamma ray (GR) log in the analysis to separate segments of the well into more homogeneous groupings based on the API value of the GR.

When calculating the standard deviation of PR and YME for defining the geomechanically homogeneous zones of the reservoir, initial gamma ray divisions included three value sets: 0-300, 300-450, and greater than 450 API. Further analysis showed a noticeable change between the reservoir at 0-300 API and the reservoir greater than 300 API. Because of the similar results found in the upper two divisions, they were combined. Analysis was evolved to include two divisions: less than 330 API and greater than 330 API. The 330 API cut off was determined

based on the gamma ray and density well logs and where they had abrupt or significant changes in values which indicated a change in the rock lithology.

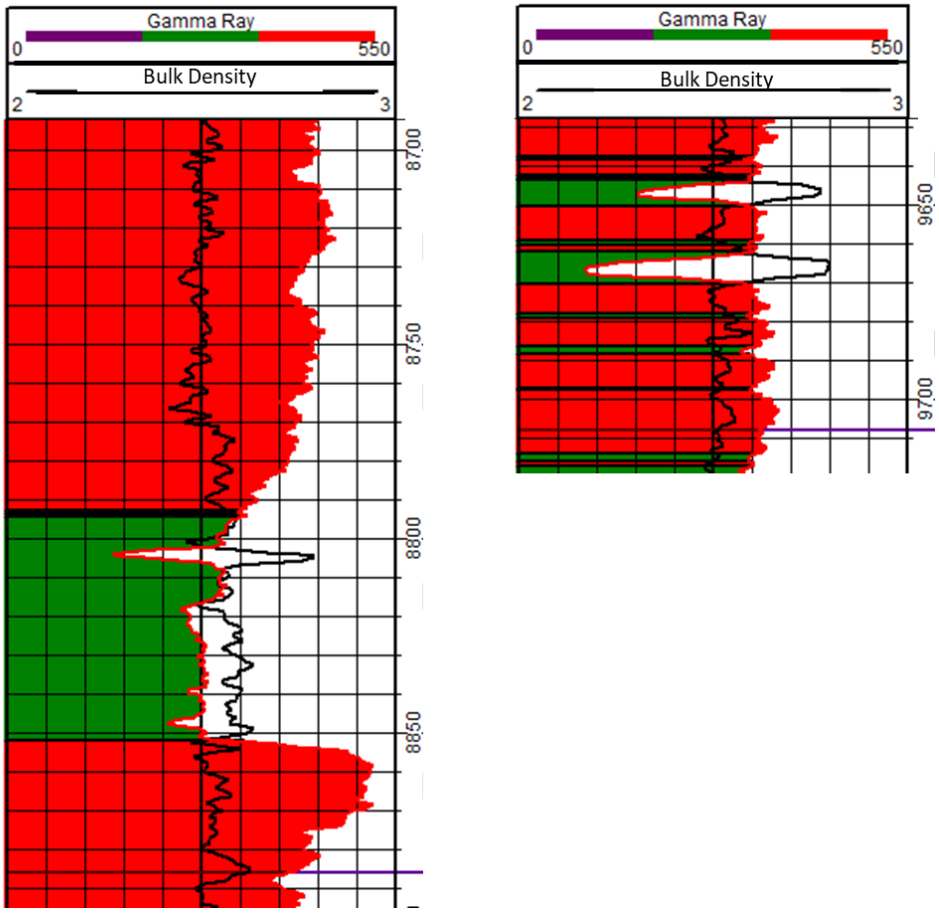

	Depths	Poisson's Ratio	Young's Modulus
Red	8700-8780	0.021	0.10
Green	8800-8500	0.025	0.30
Both	9635-9700	0.039	0.66

Figure 6 Gamma ray log with color shading green 0-330 API and red >330 API. Black line represents bulk density. An example of the standard deviation values for Poisson's Ratio and Young's Modulus for each of the gamma ray divisions.

In **figure 6,** these are represented by the colors green and red. The green shading of the gamma ray indicates that the gamma ray is less than 330 API, and the red shading represents gamma ray greater than 330 API. The values in **figure 6** give an example of the standard deviation for an

individual red zone, individual green zone, and a combination of the two. Red and green separately are considered homogeneous zones, while red and green together are heterogeneous. The calculation of standard deviation in homogeneous zones is low when compared with the standard deviation of the heterogeneous zones.

Cluster placement within the potential homogeneous or heterogeneous zones was analyzed for individual stages to determine if the gamma ray could be used to separate the well into areas of geomechanically homogenous zones that would be detailed enough to implement when placing clusters. The intention of this division of the reservoir was to determine if the gamma ray could be used to place perforations at geomechanically homogeneous locations with the goal of increasing the stimulation efficiency of each stage.

In addition to this, the mean PR and YME log values were calculated at each perforation location, and magnitude and deviation of the geomechanical moduli of clusters for each stage was analyzed. The purpose of only including the reservoir at perforation locations was to create control within the data to avoid zones of the reservoir that were potentially not impacting stage stimulation. The values of the averages and the range in the values was considered when determining factors resulting in efficient stimulation.

2.3 Natural Fracture Identification and Analysis

There are two joint sets described by Engelder et al. (2009) in the Marcellus: J1 and J2. J1 joints are crosscut by J2 and formed at, or near, peak burial of the Marcellus Shale. Burial of the Marcellus occurred during the Alleghenian orogeny in the Permian, which resulted in hydrocarbon generation from maturation of organic material. This maturation created "abnormal" pressures within the formation that caused natural fractures to form throughout the

reservoir. J1 joints are east/northeast striking and run roughly parallel to the maximum horizontal tectonic stress of the area. J1 joints are predominantly found in black shale, whereas J2 are more often found in siltstone. This, along with evidence that these joints do not intersect, or only slightly intersect, calcite concretions (McConaughy and Engelder, 1999) supports the interpretation that the J1 joints are natural hydraulic fractures and the result of hydrocarbon generation.

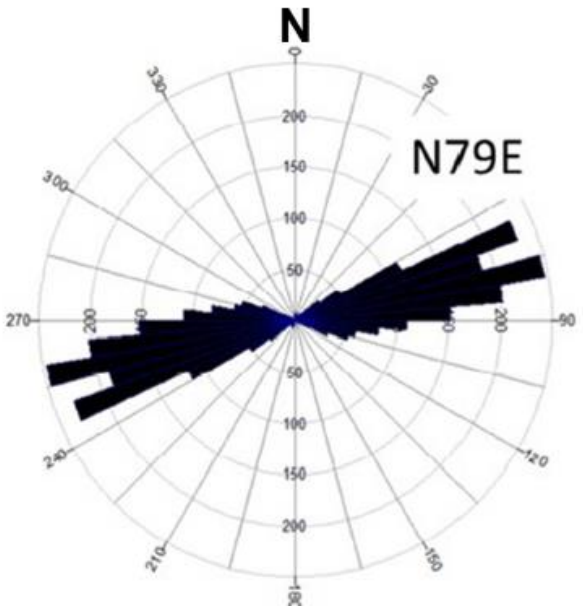

Figure 7 Rose diagram of the orientation of the strike of natural fractures along the MIP-3H well bore. The average strike at N79E.

It is beneficial for natural gas extraction from the reservoir that J1 joints or fractures run perpendicularly to the minimum horizontal tectonic stress, because horizontal wells, like the MIP-3H well, drilled in the northwest-southeast direction cut and drain J1 fractures (Engelder, 2009). Strike orientations of the natural fractures, along the MIP-3H horizontal wellbore, are represented by the rose diagram in **figure 7** and show an average northeast trend of 79 degrees. This value is comparable to the 82 degrees discussed in Engelder (2004). Fractures identified

along the horizontal well bore of the MIP-3H well are almost all calcite-filled. The number of fractures per stage of the MIP-3H well along with the measured depth of each stage are listed in **table 1.**

Natural Fracture Count per Stage

Stage	Top of Stage (ft)	Bottom of Stage (ft)	Stage Length (ft)	Number of Fractures
28	7732	7969	237	28
27	7969	8198	229	66
26	8198	8424	227	89
25	8424	8656	232	42
24	8656	8886	230	41
23	8886	9069	183	21
22	9069	9249	180	46
21	9249	9474	225	37
20	9474	9708	234	71
19	9708	9891	183	68
18	9891	10070	180	56
17	10070	10254	184	25
16	10254	10432	178	90
15	10432	10617	185	14
14	10617	10843	226	17
13	10843	11069	227	72
12	11069	11301	231	65
11	11301	11533	232	86
10	11533	11759	226	160
9	11759	11993	235	97
8	11993	12216	223	51
7	12216	12435	219	47
6	12435	12673	239	69
5	12673	12908	235	15
4	12908	13139	231	29
3	13139	13376	237	48
2	13376	13601	225	25
1	13601	13856	255	41

Table 1 Pre-existing natural fracture count for each stage in the MIP-3H well.

These fractures were identified using Schlumberger's Quanta Geo technology. Quanta Geo allows for 98% of borehole coverage in eight inch holes, measures a range of resistivity from 0.2 ohm-m to 20,000 ohm-m within the formation, and has a sampling rate of 0.2 inch when sampling at 3600 feet per hour and 0.1 inch when sampling at 1800 feet per hour (Laronga and Shalaby, 2014). The resistivity contrast between shale and calcite allowed fractures within the formation to be more easily identified. Over 1600 calcite-filled fractures were located along the lateral portion of the MIP-3H well, and the reactivation of these fractures during well stimulation is one way of creating permeability within the reservoir. Fracture failure, Mohr-Coulomb models suggest that these fractures are activated when pore pressure is increased during hydraulic stimulation (Evans et al., 2019). Petra IHS software was used to plot the distribution of fractures along the well bore along with the location of perforation clusters. This displays the fracture intensity of individual stages along the length of the MIP-3H well and allows for visualization of fracture location and intensity relative to cluster placement. Poisson's Ratio and Young's Modulus logs are included in the image and show greater deviation in stage 10 than in stage 14. The high frequency of fractures in stage 10 may be creating variation in the PR and YME values.

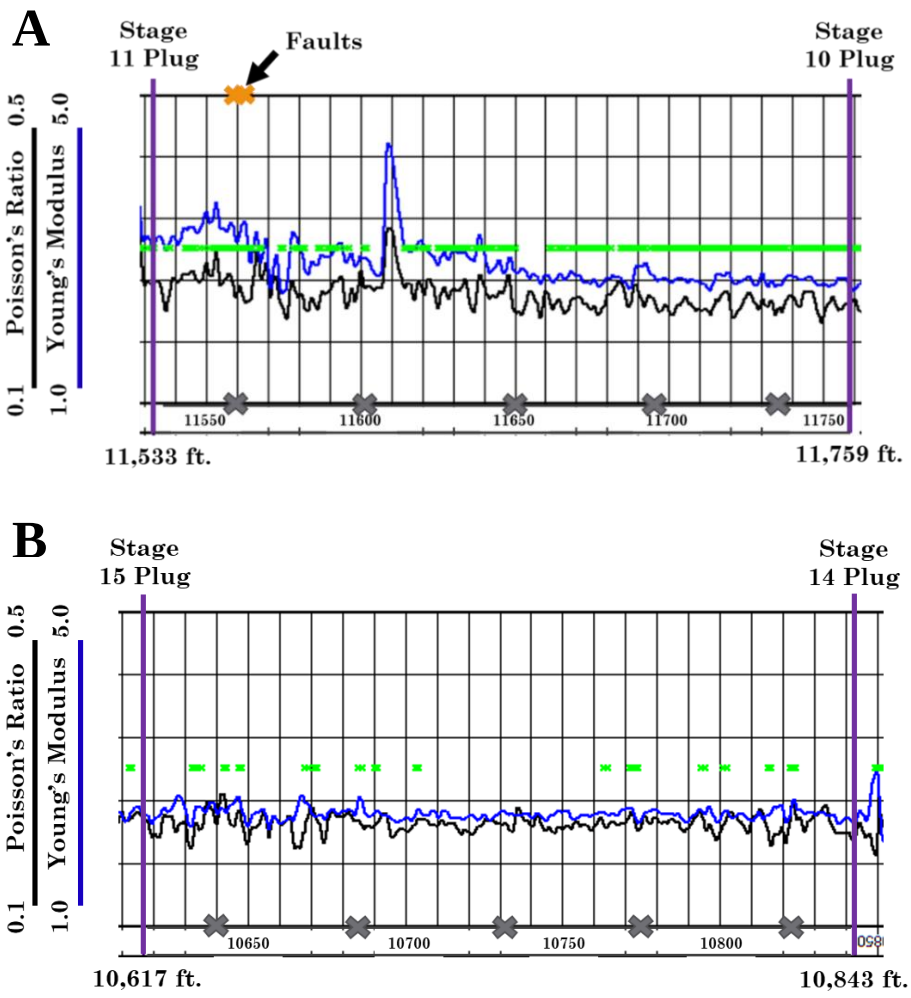

Figure 8 Fracture distributions within Stage 10 and Stage 14 of the MIP-3H well. Individual fractures are represented by a green "x", faults are represented by an orange "x", and each cluster location is indicated by gray "x". A. Stage 10 has 160 fractures and two faults. B. Stage 14 has 17 fractures picked.

Figure 8 shows how the natural fracture distribution can vary between stages. Stages 10 and 14 show how in natural fracture intensity can vary throughout the reservoir. One hundred and sixty pre-existing fractures and two faults were picked for stage 10, while only 17 fractures were identified within stage 14. The reactivation of natural fractures can have both a positive and

negative affect on stimulation and the subsequent production of stages within unconventional shale-gas wells, so it is important to consider these fractures when completing stages.

2.4 Fiber Optic Distributed Acoustic Sensing Data

The first application of DAS in a tight gas well occurred in 2009 and is a source of real time data that was difficult to obtain with technology up to that point. It is applicable as a permanent source of information that does not interfere with the operation of the well. This technology is sensitive and reliable enough to obtain data on logging operations, perforating, and hydraulic stimulation. DAS allows for the observation of individual clusters during the hydraulic fracturing process which is used to determine which clusters are taking the majority of the fracturing fluid (Molenaar et al., 2012).

The distributed acoustic sensing (DAS) laser interrogator system is a continuous process which records disturbances along the entire length of the fiber; this records any vibration or mechanical movement of the fiber. DAS data is acquired by observing the backscattering of light from each pulse of laser signal into the optic fiber. Changes in the fiber path caused by acoustic waves hitting the fiber alters the fiber structure which causes varying degrees of backscattered light. The processing system converts the collected data into differential strain which occurs due to acoustic vibration. The vibration subjects the fiber to varied levels of pressure, reflecting the varying levels of strain applied to the fiber during stimulation of the well. This is interpreted as the distribution and intensity of energy contributed to each individual cluster during hydraulic fracturing.

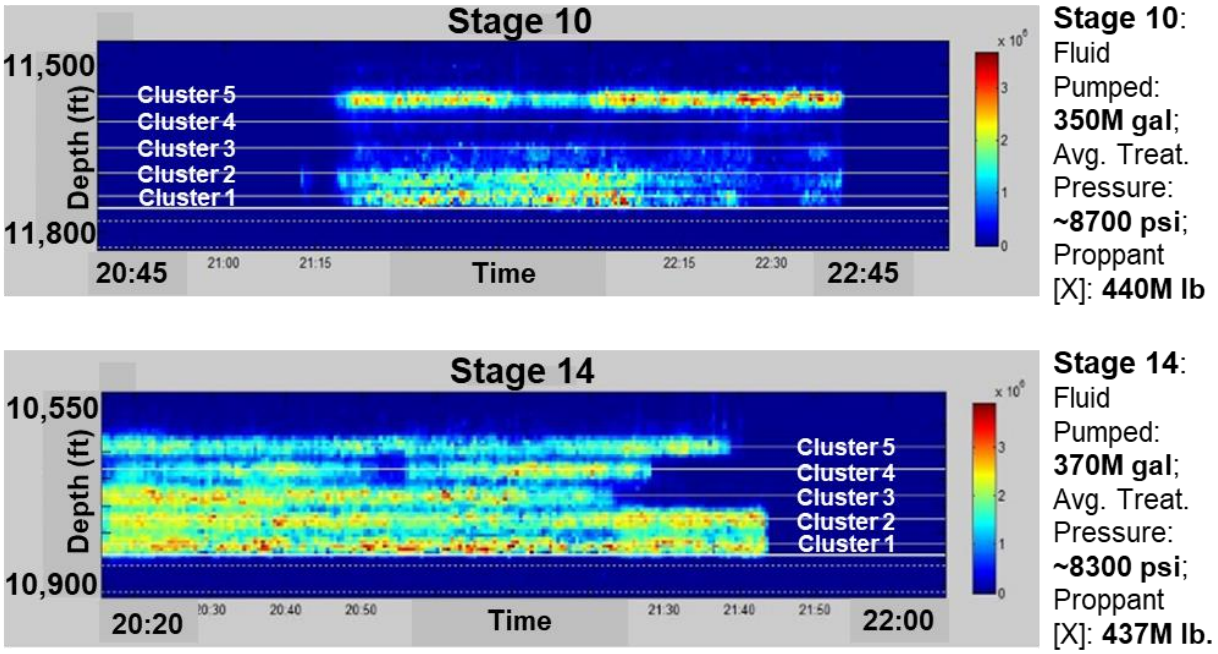

Figure 9 Stage 10 shows an uneven distribution of energy during stimulation with most of the fracturing fluid stimulating clusters one, two, and five. Stage 14 has a much more even distribution of energy across all five clusters.

Distributed Acoustic Sensing (DAS) and Distributed Temperature Sensing (DTS) fiber optic data were acquired for the MIP-3H well. Because the fiber is in place during hydraulic stimulation of the well, energy distribution and temperature changes were recorded during the completion of for individual clusters in each individual stage. DAS measures the amount of vibration during hydraulic fracturing. This shows the potential stimulation efficiency of each stage by displaying where the energy was distributed during injection of the fracturing fluid (MacPhail et al., 2012).

Figure 9 shows the distributed acoustic sensing (DAS) measurements during hydraulic stimulation of stages 10 and 14 of the MIP-3H well. Each horizontal line with a color range of blue to red is a perforated location along the stage and shows the DAS changes over the time that hydraulic stimulation occurred. Warmer colors, like reds and yellows, indicate that higher levels of strain are occurring, whereas the cooler colors, like blue, indicate lower levels of strain. As

time progresses, these DAS figures show the variation of the amount of energy that is contributed to each clusters of perforations within each stage. The geomechanical properties and fracture distribution observed for individual stages are compared to the energy dispersed during hydraulic stimulation that is represented by the DAS data. Factors contributing to efficient distribution of energy during well stimulation are identified with the use of DAS data.

3. Results and Discussion

During analysis, all outlying data that was likely the source of human error or variations in completion approaches using different proppants and chemicals were not considered for quality control. This includes completion stages 22 through 28 where multiple techniques were attempted, and stage 11 where recording issues were observed. An inconsistency between data sets was found at stages 22 and 23 that was reported as two sets of completion data, one indicating four cluster locations and another indicating five clusters for these two stages. The variance in this data resulted in a shift in the measured depths reported for stages 22 through 28. The DAS data for stage 11 appeared to be unreliably recorded and is not a trusted source for stage stimulation. For the purpose of quality control, these stages were not included in the analysis.

Geomechanical properties, pre-existing fracture distribution, and minimum horizontal stress are compared to the amount of strain, or the energy experienced, at each completion cluster that is provided by the fiber optic distributed acoustic sensing (DAS) data. The “evenness” of the energy distribution is related to the efficiency of stimulation for each stage. Stages 2 through 21 are separated into two main groups: even and uneven energy distribution.

The DAS data in **figure 10** shows comparatively even distribution of energy during stimulation for stages 9, 13-19, 20, and 21. These stages are designated as Group A. **Figure 11** shows the uneven distribution of energy in stages 2-8, 10, and 12, so these stages are labelled Group B. Stage 20 shows even distribution in clusters 2-5, while no strain on the fiber occurred at cluster 1. The lack of energy to cluster 1 for stage 20 is interpreted as a result of an ineffective cluster, so the stage will be included in the Group A. Perforations for stage 17 were placed into two longer length clusters rather than four or five. This explains why DAS data only shows energy distributed to two locations along the stage.

GROUP A

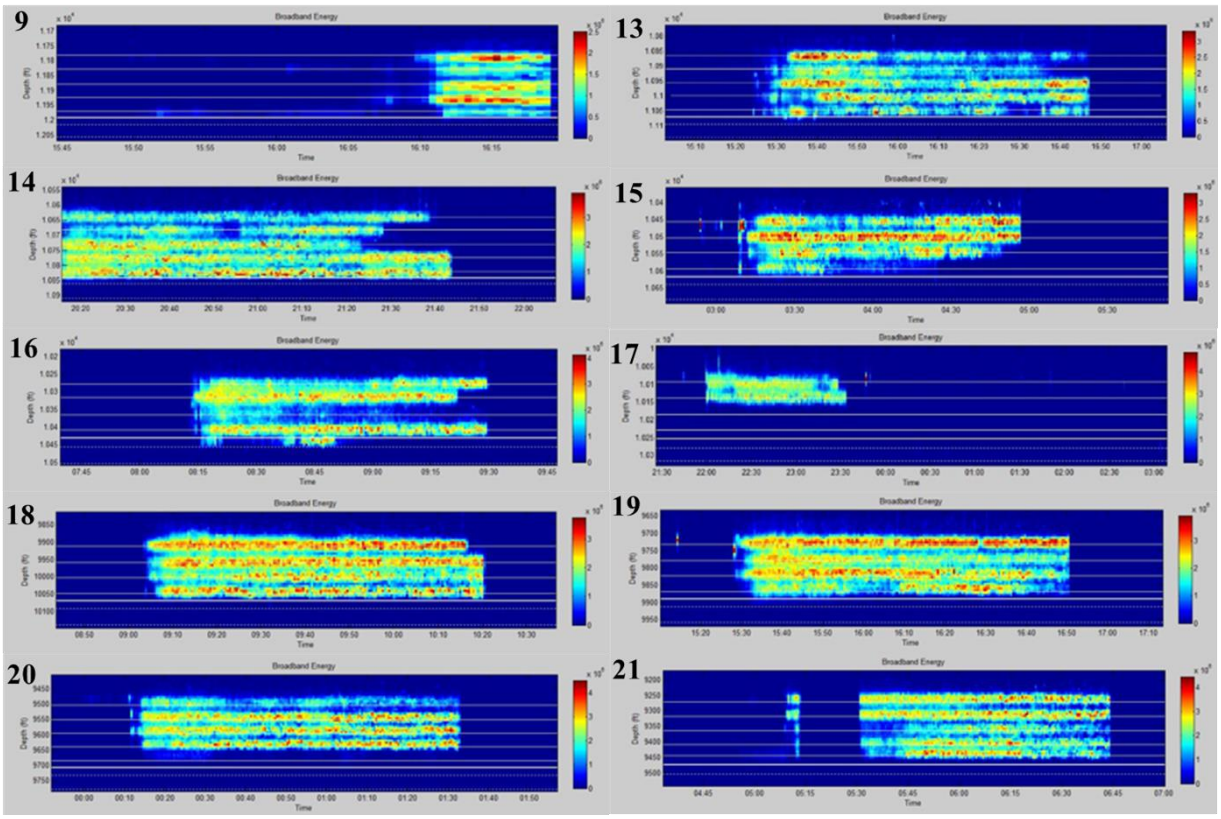

Figure 10 Group A: DAS data showing even energy distribution during the hydraulic fracturing of stages 9, 13, 14, 15, 16, 17, 18, 19, 20, and 21. Red indicates high levels of strain on the fiber while blue represents little to no strain. The initial horizontal line at the bottom of each image is the plug location, and each line above that showing strain on the optic fiber is a cluster within that stage. The x-axis is time, and the y-axis is measured depth. The y-axis read upward is toward the heel of the well.

GROUP B

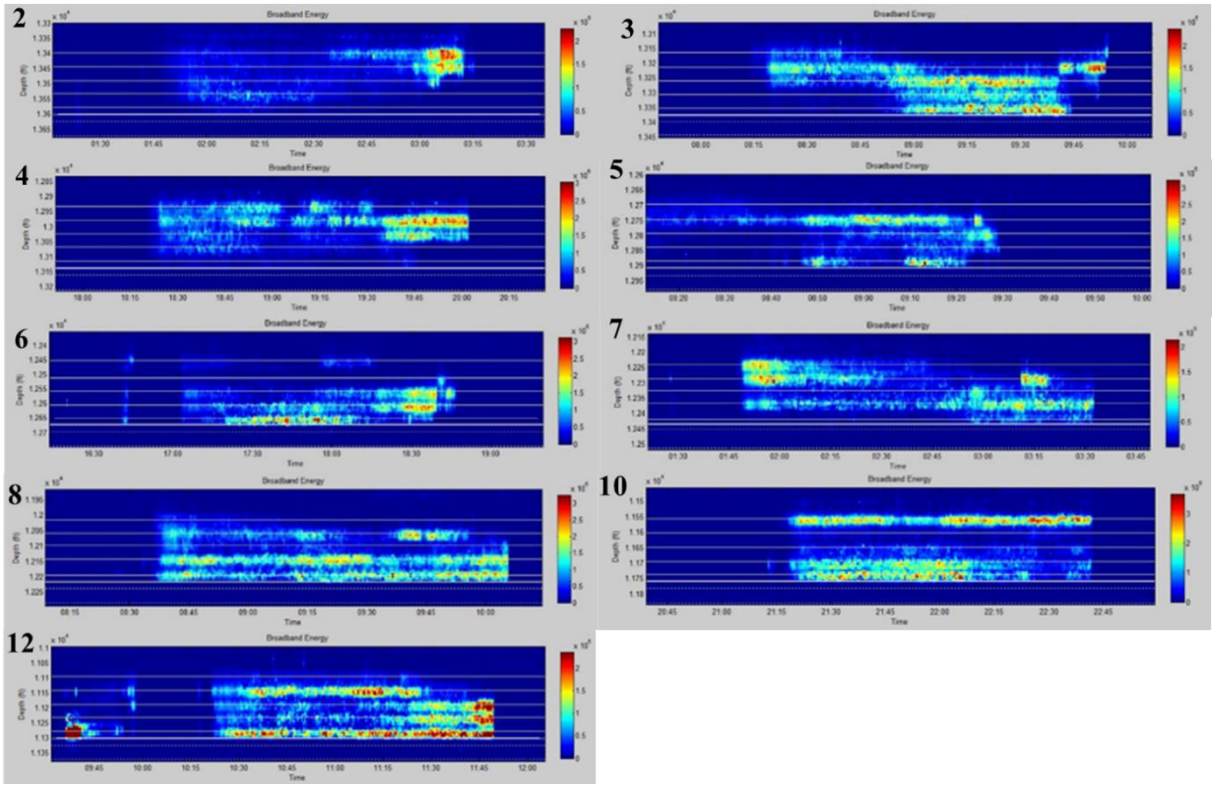

Figure 11 Group B: DAS data showing uneven energy distribution during hydraulic fracturing of stages 2, 3, 4, 5, 6, 7, 8, 10, and 12. Red indicates high levels of strain on the fiber while blue represents little to no strain. The initial horizontal line at the bottom of each image is the plug location, and each line above that showing strain on the optic fiber is a cluster within that stage. The x-axis is time, and the y-axis is measured depth. The y-axis read upward is toward the heel of the well.

3.1 Geomechanical Moduli: Poisson's Ratio and Young's Modulus

3.1.1 Results

The placement of clusters within homogeneous vs. heterogeneous zones defined by the gamma ray magnitude was compared to the distribution of energy to those clusters. The gamma ray (GR) was separated into two divisions: less than 330 API and greater than 330 API. Gamma ray less than 330 API was assigned green, and GR greater than 330 API was assigned red. If perforation clusters did not clearly have a GR of green or red, then they were labelled as "both". The purpose of this was determine if geomechanically homogeneous zones could be found based on GR

magnitude and then applied when placing perforations. The standard deviation of Poisson's Ratio and Young's Modulus was relatively low in the red and low in the green, but when red and green were combined, there was an increase in the standard deviation values.

The overall goal was to determine if GR could be used to define geomechanically homogeneous zones for the placement of perforation clusters in order to lead to more efficient and even distribution of energy during hydraulic stimulation of the stage. The only constant variation in values was generated when comparing thick "red zones" to "green zones". Though there was a noticeable change between these, there was no connection between similar GR and similar geomechanical values once above the 330 API cutoff. Results showed there were no clear connections between the geomechanically homogeneous stages created through GR separation and even energy distribution during stage stimulation. For example, twelve of the nineteen stages included in the study were completed exclusively in zones of the reservoir with GR values higher than 330 API. Of these twelve stages, six of them were in Group B and six in Group A. The application of GR for separating geomechanically heterogeneous stages from homogeneous stages with the goal of generating even hydraulic stimulation does not yield consistent efficient stimulation results.

When creating the Poisson's Ratio (PR) and Young's Modulus (YME) cross-plots for the completion stages in the MIP-3H well, the length of the well from plug to plug was included to determine if a trend could be identified. **Figure 12** and **13** show the cross-plots of stages 2 through 21, excluding stage 11. **Figure 12** is the grouping of evenly stimulated stages, Group A, and **figure 13** shows Group B, the unevenly stimulated stages. In these figures, Young's Modulus is on the y-axis and Poisson's Ratio is on the x-axis. The red lines are used to indicate the general transition of high to low brittleness for PR and the change in rigidity in YME that is

described by Grieser and Bray, 2007. The z-axis was used to represent the measured depth of each data point to see if there were noticeable geomechanical changes within a stage with increasing or decreasing depth. Stage 10 had consistent geomechanical change with depth, but this was not seen in other stages.

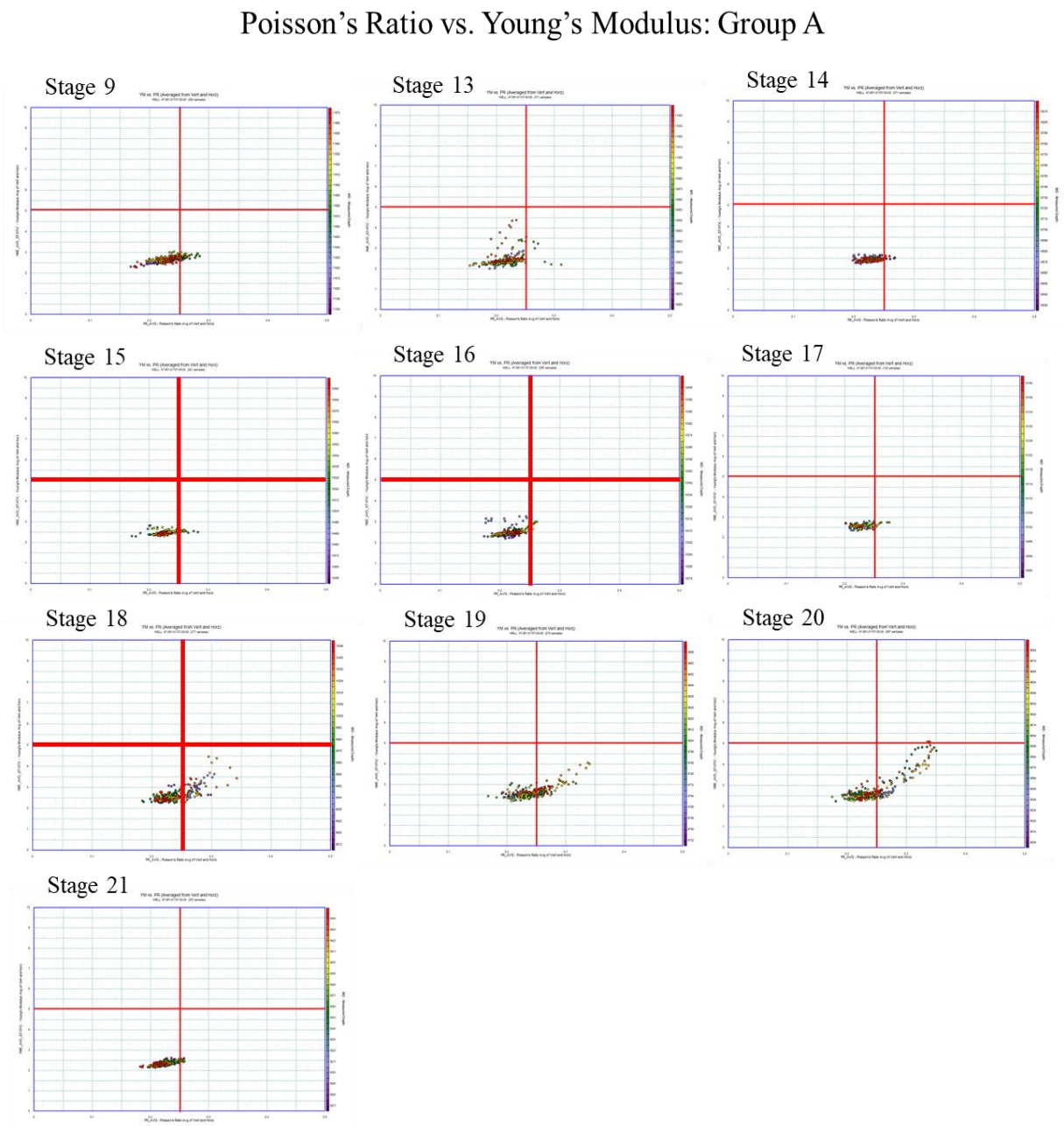

Figure 12 Poisson's Ratio vs. Young's Modulus cross-plot for stages of even DAS. Stages included are 9, 13, 114, 15, 16, 17, 18, 19, 20, and 21. Poisson's ratio is on the x-axis and has a scale of 0.1 to 0.5. Young's Modulus is on the y-axis and has a scale of 0.0 to 10.0. The vertical, red line crosses the x-axis at 0.25 and the horizontal, red line crosses the y-axis at 5.0.

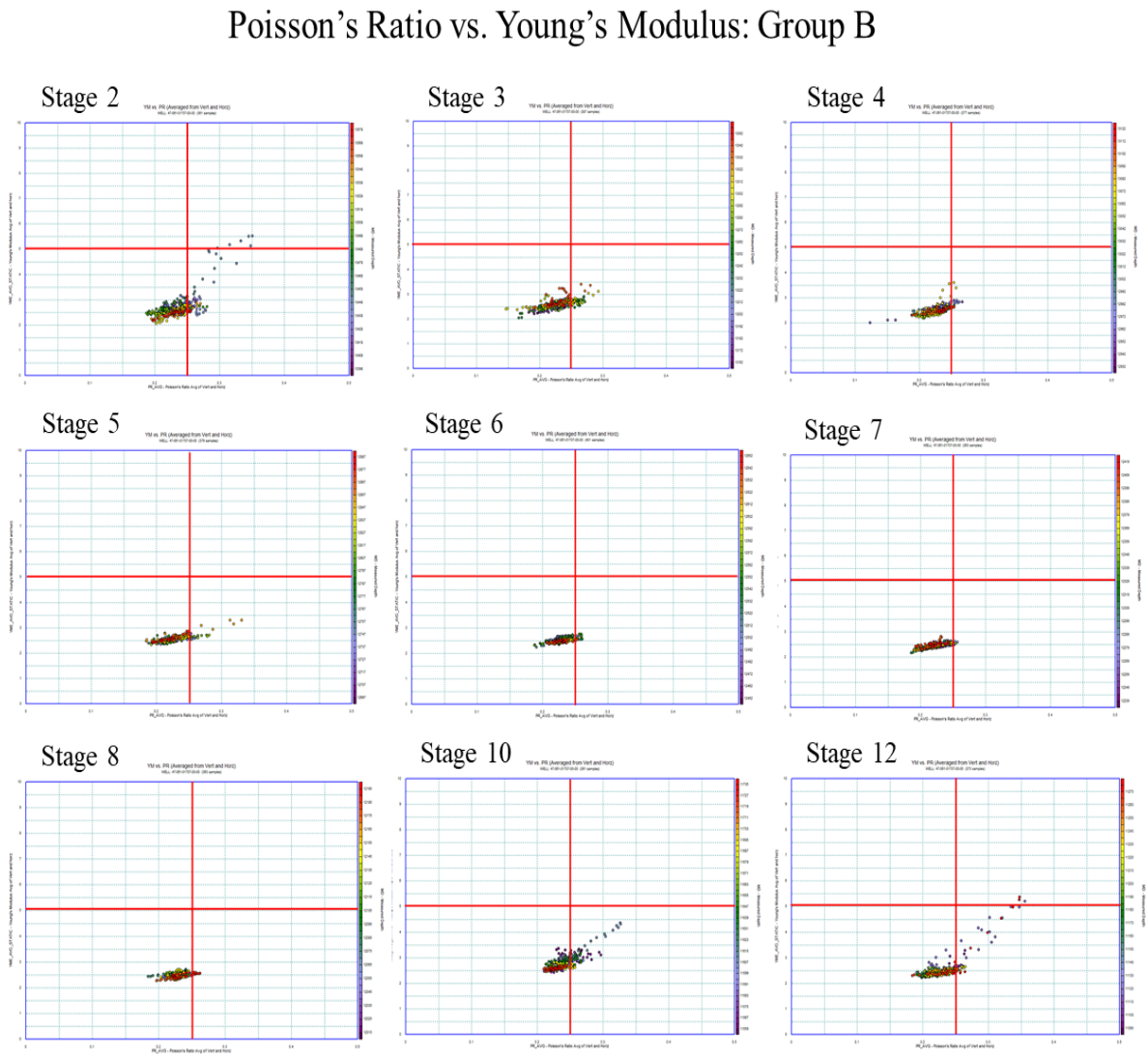

Figure 13 Poisson's Ratio vs. Young's Modulus cross-plot for stags with uneven DAS. Stages included are 2, 3, 4, 5, 6, 7, 8, 10, and 12. Poisson's Ratio is on the x-axis and has a scale of 0.1 to 0.5 Young's Modulus is on the y-axis and has a scale of 0.0 to 10.0. The vertical, red line crosses the x-axis at 0.25 and the horizontal, red line crosses the y-axis at 5.0.

Examination of these cross-plots did not show consistent changes between Group A and Group B stages. The bulk of the reservoir rock is comparatively similar when placed against lithologies with higher calcite or silica content. Variations in the data are difficult to pick out and analyze from cross-plots of the Marcellus Shale data set. Because of this, looking at the specific geomechanical values is more applicable. To do that, the average, or mean, was calculated for the reservoir at each perforation cluster. When calculating the mean values for PR and YME,

including the entire stage would result in data points that potentially have no effect on stimulation, so in order to have a constant data set and to avoid irrelevant data points from impacting the results, only log data obtained at completion clusters was included in the calculations.

Poisson's Ratio (PR) values for evaluating brittleness can range from 0.1 to 0.5 with the general transition from brittle to malleable occurring around 0.25 according to Grieser and Bray, 2007. The PR of the clusters within the Marcellus MIP-3H well ranged from ~ 0.19 to ~ 0.33. **Table 2** lists the mean values of Poisson's Ratio for stage 2 through stage 21. Stages with a Poisson's Ratio (PR) range of 0.02 or less between all clusters are stages 8, 14, 15, 16 17, 18, and 19. All but stage 8 are included in Group A in **figure 10** and experience even energy distribution during stimulation which gives ~ 86% of stages experiencing efficient stimulation when PR values have minimal variation. When observing stages with a range of 0.03 or greater in the PR values of clusters, three of the nineteen (~ 16%) were Group A and nine of nineteen (~ 47%) were from Group B. On average, uneven energy distribution is linked with a greater range of Poisson's Ratio values. There was no link between lower PR values, or more brittle reservoir rock, and increased stimulation energy. Within stages, energy from hydraulic fracturing did not preferentially take the path of more brittle clusters.

Mean Values of Poisson's Ratio per Cluster					
STAGES	CLUSTER 1	CLUSTER 2	CLUSTER 3	CLUSTER 4	CLUSTER 5
Stage 2	0.23	0.21	0.20	0.27	0.23
Stage 3	0.22	0.21	0.23	0.23	0.20
Stage 4	0.23	0.22	0.23	0.26	0.24
Stage 5	0.21	0.23	0.21	0.25	0.23
Stage 6	0.22	0.23	0.25	0.22	0.24
Stage 7	0.23	0.22	0.22	0.23	0.20
Stage 8	0.23	0.23	0.24	0.22	0.23
Stage 9	0.24	0.24	0.23	0.23	0.21
Stage 10	0.22	0.22	0.22	0.25	0.26
Stage 11	0.26	0.25	0.22	0.22	0.22
Stage 12	0.33	0.22	0.21	0.23	0.26
Stage 13	0.24	0.23	0.22	0.19	0.23
Stage 14	0.25	0.23	0.23	0.23	0.24
Stage 15	0.22	0.22	0.20	0.22	XX
Stage 16	0.23	0.21	0.22	0.21	XX
Stage 17	0.22	0.23	0.23	0.23	XX
Stage 18	0.22	0.23	0.23	0.22	XX
Stage 19	0.27	0.24	0.25	0.25	XX
Stage 20	0.23	0.22	0.20	0.27	0.23
Stage 21	0.19	0.23	0.24	0.22	0.22

Table 2 Average Poisson's Ratio values of each cluster per stage of the MIP-3H well. Cluster 1 is located at the toe end of the stage and cluster 5 at the heel.

Mean Values of Young's Modulus per Cluster (Mpsi)					
STAGES	CLUSTER 1	CLUSTER 2	CLUSTER 3	CLUSTER 4	CLUSTER 5
Stage 2	2.51	2.12	2.44	2.55	2.66
Stage 3	2.66	2.44	2.58	2.57	2.31
Stage 4	2.45	2.56	2.43	2.78	2.63
Stage 5	2.53	2.54	2.62	2.56	2.58
Stage 6	2.49	2.51	2.69	2.54	2.63
Stage 7	2.56	2.43	2.42	2.45	2.40
Stage 8	2.41	2.67	2.59	2.45	2.56
Stage 9	2.68	2.67	2.62	2.56	2.48
Stage 10	2.54	2.60	2.72	2.84	3.26
Stage 11	3.12	2.74	2.44	2.60	2.44
Stage 12	4.83	2.37	2.29	2.43	2.65
Stage 13	2.48	2.39	2.32	2.32	2.32
Stage 14	2.53	2.37	2.44	2.47	2.47
Stage 15	2.40	2.69	2.69	2.47	XX
Stage 16	2.53	2.46	2.46	2.31	XX
Stage 17	2.59	2.59	2.52	2.52	XX
Stage 18	2.41	2.47	2.56	2.57	XX
Stage 19	2.84	2.56	2.48	2.50	XX
Stage 20	2.38	2.39	2.59	2.69	2.54
Stage 21	2.18	2.31	2.48	2.30	2.37

Table 3 Average Young's Modulus values of each cluster per stage of the MIP-3H well. Cluster 1 is located at the toe end of the stage and cluster 5 at the heel.

The average values of Young's Modulus at each cluster are found in **table 3.** The calculated mean values of Young's Modulus (YME) ranged from ~ 2.12 to ~ 4.83 Mpsi, but the majority of the data falls between 2.10Mpsi and 2.85 Mpsi. Young's Modulus does not vary throughout the reservoir as much as Poisson's Ratio. Values less than ~2.80 have an unremarkable effect on energy experienced at clusters. Very similar YME magnitudes exist for the majority of both Group A and Group B. There are two clusters, one in stage 10 and one in stage 12, that have abnormally high YME values. In stage 10, it is the fifth cluster, and that cluster experiences a high level of vibration during stimulation. The same is true for cluster one with high YME in stage 12. Overall, there was no change in the stimulation of stages unless the YME had a value greater than 3.00.

3.1.2 Discussion

The Marcellus Shale reservoir at this location for the MIP-3H well has a relatively small range of geomechanical values. Smaller PR indicates a more brittle material, and it is expected that that smaller values would increase the "fracability" of the reservoir resulting in more effective stimulation of those areas with smaller PR values. Even distribution of energy during stimulation occurs when PR is similar in value for each cluster within the stage. Having PR constant cluster to cluster was noticeably effective at keeping energy evenly distributed across the stage. Relatively lower PR values did not necessarily result in greater strain from stimulation.

One factor that may contribute to the relatively high energy introduced to cluster five in stage 10 is the high intensity of fractures which will be discussed later in the results section. Higher YME is expected to facilitate fracturing within the reservoir and may be the cause of the increased energy to the cluster 5 in stage 10 and cluster 1 in stage 12. These clusters have YME values noticeably higher that the other four clusters in each of those two stages. It is likely that the

higher values come from an increase in calcite content. This could be an effect of the calcite-filled fractures.

It is most likely that the method of gamma ray separation was valid when comparing the two extremes (greater and less than 330 API) because those GR values were the result of a lithology change between calcite and shale. Though this method of attempting to divide geomechanical values into homogeneous groupings with low standard deviation by gamma ray was unsuccessful, from the results of comparing Poisson's Ratio of clusters to DAS, it is still important that perforations are placed in geomechanically homogeneous zones.

3.2 Natural Fracture Distribution

3.2.1 Results

The natural fracture count per stage is shown in **figure 14**. There is no consistent tie between high fracture count for the entire stage length and the stimulation efficiency of the stage, so the analysis was adjusted to observe the location of the natural fractures in relation to the placement of perforation clusters. IHS Petra software was applied in **figure 15** and **figure 16** displays the distribution of natural fractures within each stage. For these figures, PR in black and YME in blue were included. The scale for PR is 0.1 to 0.5, and the scale for YME is 1.0 to 5.0. Young's Modulus did not exceed 5.0 in this location of the Marcellus. The scales were held constant for each of the Petra figures created for each completion stage. In each figure, the toe of the well is to the right, and clusters read in increasing order from right to left. Cluster placement is designated by navy blue rectangles at the bottom of each track image. Each green dot on the

track indicates a natural fracture picked along the lateral well bore. Stages 5, 6, and 10 each have faults picked which are indicated by an orange x at the top of each track image.

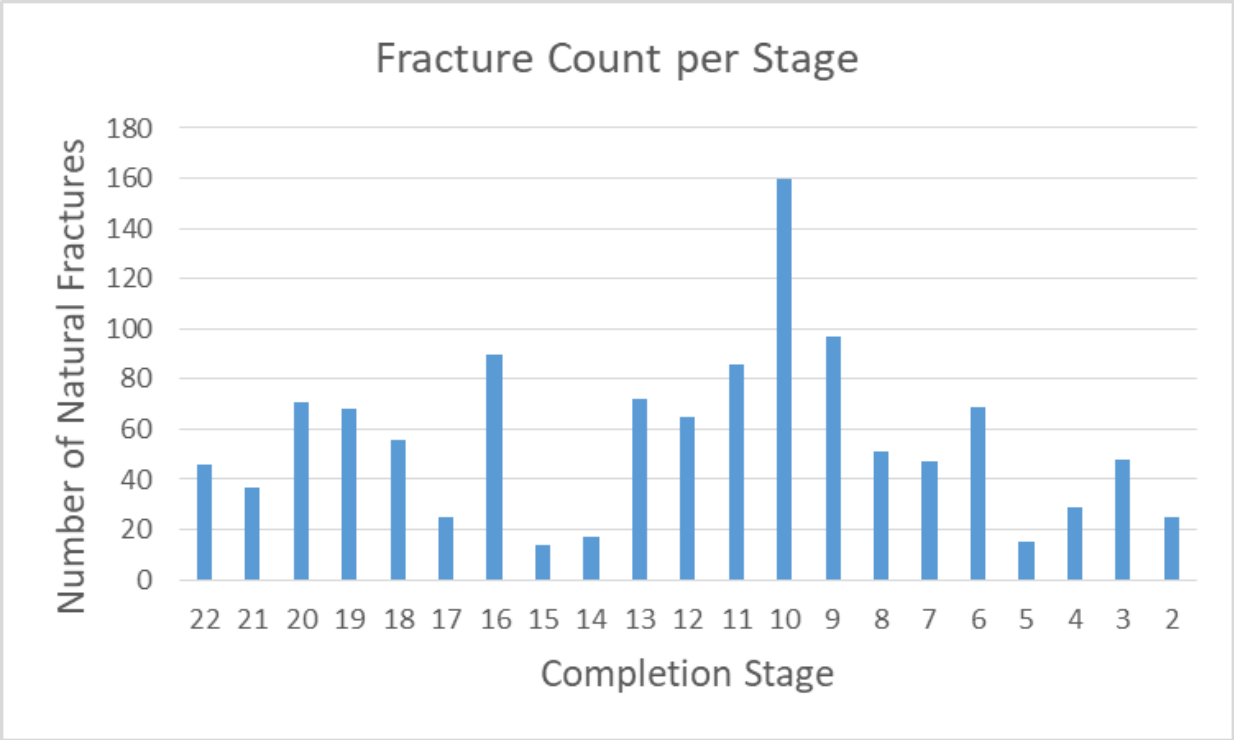

Figure 14 Number of natural fractures counted using image logs for each completion stage.

The purpose of analyzing this data was to determine if the number of fractures at each perforation cluster impacts the stimulation efficiency of the stage. This was especially important because of the results seen in stage 10 which had very high fracture intensity at clusters 1, 2, and 5 along with the presence of faults near cluster 5. This correlated to significantly more energy applied to those three clusters during stimulation. Stage 12 also showed high fracture intensity at cluster 1 along with high strain reported in the DAS at that cluster. Stage 20 had higher energy levels at clusters 2, 3, and 4 which coincided with higher natural fracture count than was present at cluster 5 in stage 20. Though stage 16 had comparatively more even energy distribution during stimulation, an analysis of fracture intensity in stage 16 shows that clusters 3 and 4 are highly

fractured compared to the other three clusters within the stage. The DAS for stage 16 also showed higher strain on the fiber at the clusters with higher pre-existing fracture counts. Apart from stages 10, 12, 16, and 20, there were no obvious variations in the stimulation of stages with regard to the fracture distribution and cluster placement. This could be because there were comparatively few highly fractured stages in the MIP-3H.

Fracture Distribution per Completion Stage: Group A

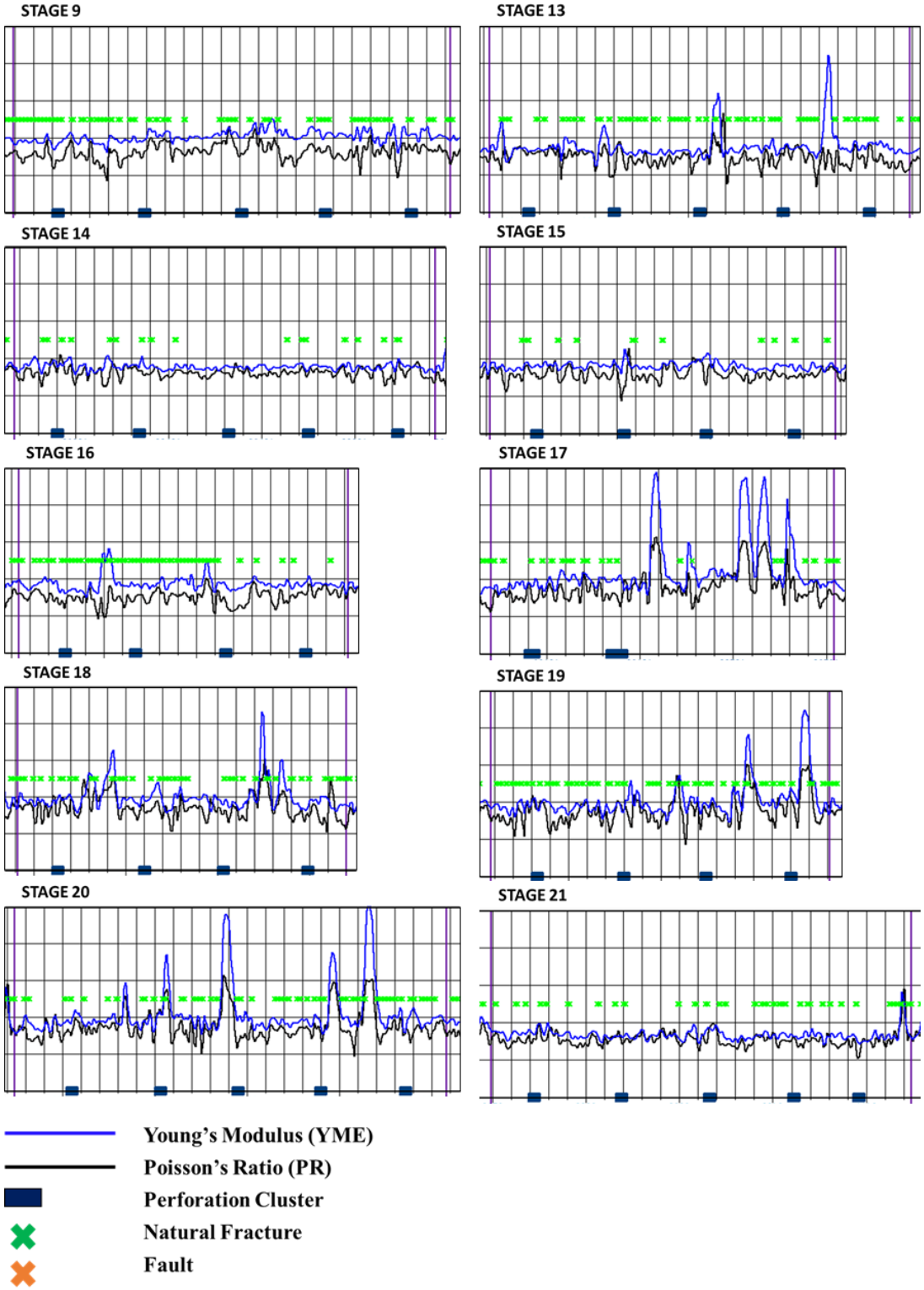

Figure 15 Group A: Natural fracture distribution in stages 9, 13, 14, 15, 16, 17, 18, 19, 20, and 21. Fractures are represented by green dots and faults by orang x's. Toe of the well is to the right in each figure. Poisson's Ratio has a scale of 0.1 to 0.5, and Young's Modulus has a scale of 1.0 to 5.0.

Fracture Distribution per Completion Stage:
Group B

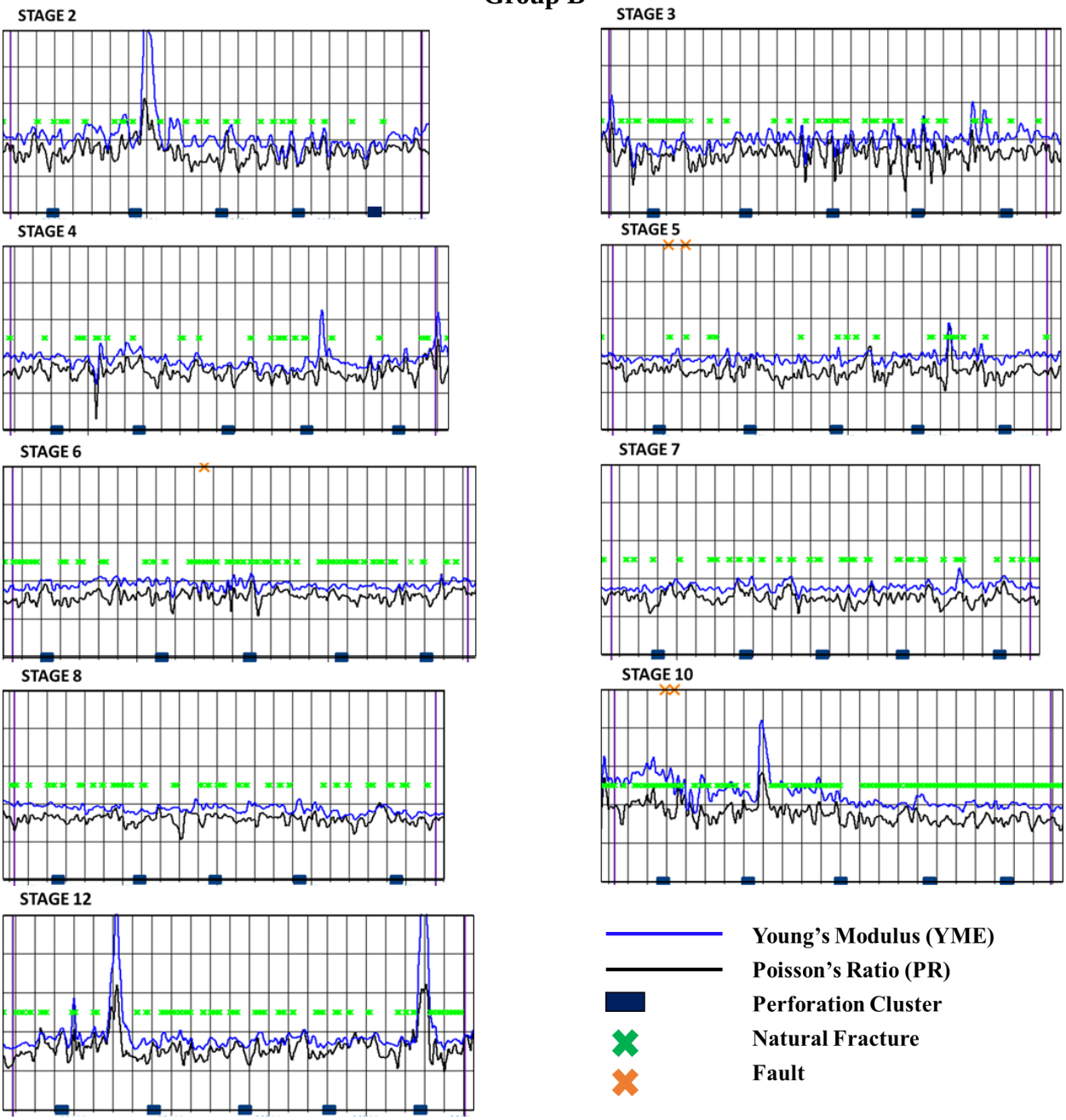

Figure 16 Group B: Natural fracture distribution in stages 2, 3, 4, 5, 6, 7, 8, 10, and 12. Fractures are represented by green dots and faults by orang x's. Toe of the well is to the right in each figure. Poisson's Ratio has a scale of 0.1 to 0.5, and Young's Modulus has a scale of 1.0 to 5.0.

3.2.2 Discussion

Results showed that high intensity of fractures at a cluster location, especially in contrast to the other clusters within the stage, will likely impact the efficiency of stimulation for that stage. Fracturing fluid will preferentially take the path of the pre-existing fractures rather than a path where induced fracturing is required. Examples of this were seen in stages 10, 12, 16, and 20. The distribution of energy observed in cluster 1 of stage 12 also showed spikes in Poisson's Ratio and Young's Modulus values. This could have been the result of an increase in calcite which would increase the moduli values. Drilling through a thick section of calcite could have obscured the presence of natural fractures. Because the resistivity contrast assists with picking fractures in this area of the Marcellus Shale, fractures in zones with higher calcite content would have been difficult to identify. "Hidden" fractures would increase the count of fractures which would increase the likelihood that fractures impacted the efficiency of stimulation for stage 12. This spike in moduli values is also seen near clusters 2, 3, and 4 in stage 20 as well as increased energy to these three clusters. It is possible that natural fractures are "hidden" at these locations. Data analysis of stage 10 showed no clear correlations between the other methods applied to this data and the DAS distribution of energy, so it is most likely that the fracture intensity and fault presence directed the fracturing fluid to clusters 1, 2, and 5. It is likely stage 12 had the same result. In the DAS data of stage 16, it appears that clusters 4 and 5 may have significant communication during stimulation. This may be due to high frequency of natural fractures creating more complex network connections between the two perforated locations.

Based on the results seen in stage 10 as well as the other stages discussed, it is very likely that cluster placement in highly fractured zones can impact the stimulation of the stage. It appears

that when stages have minor fracture counts, stimulation is neither negatively nor positively impacted when that efficiency is determined from DAS energy distribution data.

3.3 Minimum Horizontal Stress

Minimum horizontal stress (Sh_{min}) was analyzed using the mean values of the reservoir at each cluster of perforations. These average values are listed in **table 4** for stage 2 through stage 21. The seventh column (DAS Group) is referring to the two groups, A and B, which were designated based on the energy distribution shown in the distributed acoustic sensing (DAS) figures. The Sh_{min} magnitudes range from ~ 6164 psi to ~ 7616 psi with the majority falling between 6400 and 7000 psi.

STAGE	Cluster 1	Cluster 2	Cluster 3	Cluster 4	Cluster 5	DAS Group
2	6738	6413	6312	7178	6544	B
3	6501	6403	6599	6748	6209	B
4	6729	6533	6662	6953	6765	B
5	6505	6641	6404	6841	6672	B
6	6585	6622	6819	6569	6904	B
7	6781	6606	6591	6667	6362	B
8	6708	6772	6800	6560	6709	B
9	6746	6754	6636	6707	6530	A
10	6638	6617	6569	6997	6912	B
12	7616	6569	6506	6780	7010	B
13	6779	6657	6612	6164	6643	A
14	6855	6681	6698	6749	6767	A
15	6586	6608	6465	6653	X	A
16	6725	6440	6579	6403	X	A
17	6632	6746	6746	6746	X	A
18	6644	6749	6798	6656	X	A
19	7097	6944	7000	6996	X	A
20	6749	6718	6406	7243	6724	A
21	6273	6715	6898	6601	6691	A

Table 4 Average minimum horizontal stress at each perforation cluster for stages 2 through 21 (excluding stage 11).

3.3.1 Results

The comparison of minimum horizontal stress magnitudes to the energy distribution during hydraulic fracturing of the reservoir showed a clear connection between stages with homogeneous Sh_{min} values at each perforation location and an even distribution of energy during stimulation. The variation between Group A and Group B can be seen in **figure 17** which gives a graphical representation of the Sh_{min} values of each cluster. The y-axis is labeled 6200 psi to 7300 psi, and the x-axis labels each cluster. **Figure 17a** has Group A with even DAS distribution, and **figure 17b** shows Group B with uneven distribution. Sh_{min} in pounds per square inch (psi) is on the y-axis and is held constant for each stage from 6200 psi to 7300 psi. The graphs are separated into the Groups A and B referenced above. Stages completed in areas of similar Sh_{min} will generate a more horizontal line, while stages with more varied Sh_{min} values will generate a more uneven line. Less vertical change for the line graphed means less change in Sh_{min} for each of the perforated zones of the stage.

The graphs generated show a clear change between stages in Group A and stages in Group B with the slight exception of stage 16. Clusters within stage 16 have more of an overall variation in Sh_{min} values than other stages in Group A, but the Sh_{min} heterogeneity is tied to a comparatively uneven distribution of energy when related to the other stages in Group A. Stage 9, 14, 18, and 19 show very efficient stimulation in the DAS and have very little variation in Sh_{min} magnitudes. In contrast, stages 2, 3, 4, 5, 6, and 7 have significant variation in the Sh_{min} magnitudes at the perforation clusters and are tied to uneven energy distribution during stimulation.

Figure 17 Minimum horizontal stress placed on the y-axis with each cluster along the x-axis. a: Group A stages with even DAS including 9, 13, 14, 15, 18, 16, and 19. b: Group B stages with uneven DAS including 2, 3, 4, 5, 6, 7, and 10.

A direct relationship between Poisson's Ratio and the minimum horizontal stress magnitude was observed. This is shown in the cross-plot in **figure 18a.** Poisson's ratio is placed on the y-axis with Sh_{min} on the x-axis. Poisson's Ratio values correlate to minimum horizontal stress values, and the trend line of the data points has an R-squared value of ~ 0.93. When values of PR were constant, Sh_{min} at those same locations had a similar result. For this reason, stages that were determined to be homogeneous based on the Poisson's Ratio data overlap with stages that have similar minimum horizontal stress magnitudes for each cluster. Young's Modulus was also placed against Sh_{min} in a cross-plot which is shown by **figure 18b.** There is less of a trend in the data when compared with the Poisson's Ratio cross-plot, and the R-squared value from YME is ~0.39.

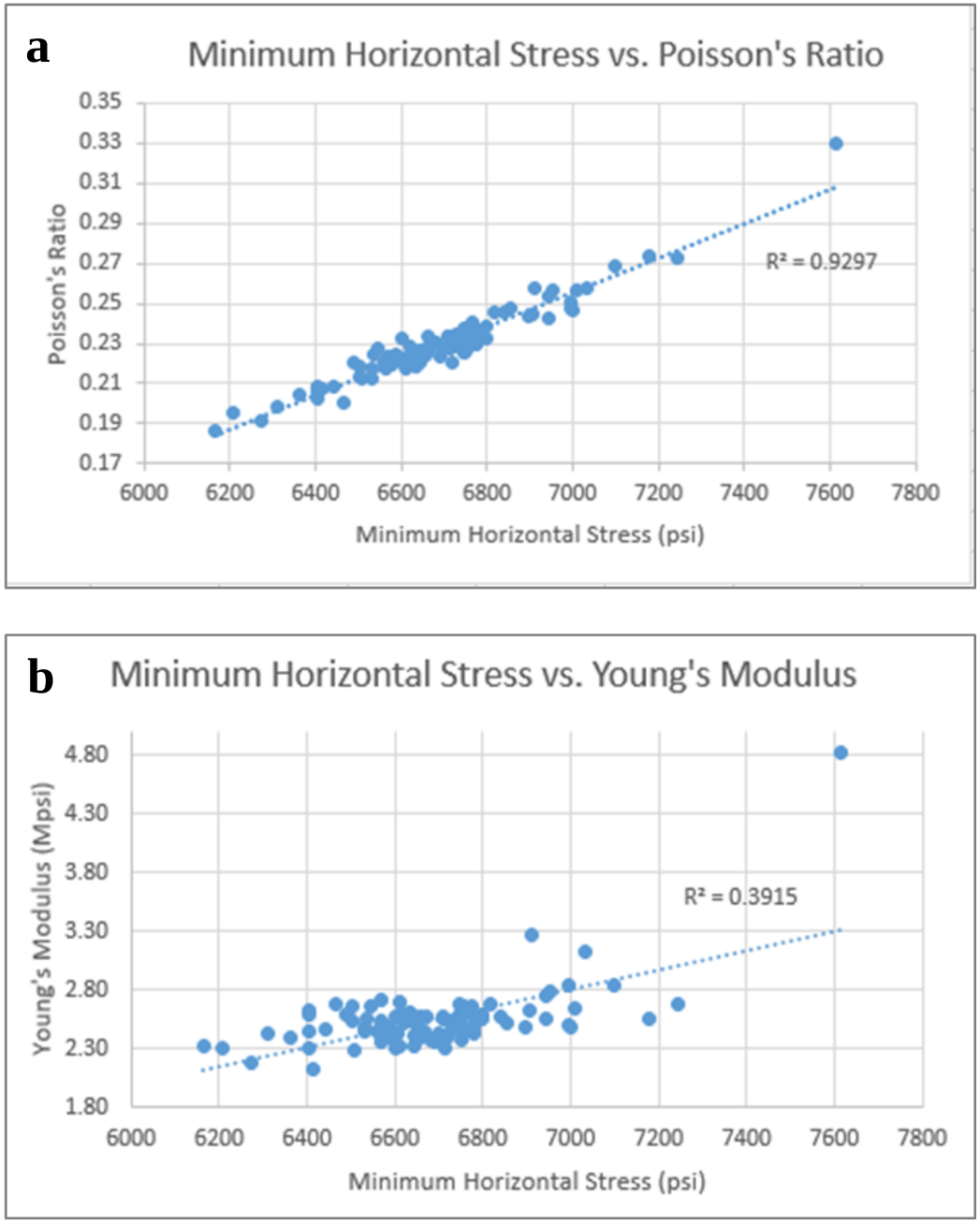

Figure 18 Cross plot of geomechanical moduli, Poisson's Ratio and Young's Modulus, with the minimum horizontal stress. a: trend between minimum horizontal stress and PR b: trend between minimum horizontal stress and YME.

3.3.2 Discussion

It is likely that smaller minimum horizontal stress magnitudes will result in a more "fracable" reservoir, but analysis of the efficiency of stimulation with the magnitudes of minimum horizontal stress show that keeping the Sh_{min} relatively equal for each cluster is more effective in generating even DAS rather than focusing on perforating the lowest Sh_{min} values. Optimal conditions for inducing fractures within the reservoir are likely clusters placed in zones of small but equal Sh_{min}. Smaller Sh_{min} values would be more likely to allow fracture propagation perpendicular to the wellbore, but stages with even distribution of energy shown in the DAS tended to have like Sh_{min} values regardless of where they fell in the 6400 psi to 7100 psi range.

Though there is a noticeable overlap in the results found from both the Poisson's Ratio and Sh_{min} analyses, when determining homogeneous reservoir zones for cluster placement, Sh_{min} would likely be a more effective method than using only PR. Sh_{min} takes into account many variables that create heterogeneity within the reservoir which include Poisson's Ratio as well as vertical stress, Biot's Coefficient, and pore pressure.

Though this was the most common result, there are examples where even DAS did not correlate with Sh_{min} such as stages 16 and 21.These stages have relatively broad ranges of Sh_{min} values but still resulted in comparatively even DAS data. This could be the impact of other factors such as the natural fracture distribution discussed earlier in the paper. Of the stages showing even energy distribution, it seems that having only one cluster varying by ~ 200 psi or greater did not significantly impact the stimulation efficiency. This is seen in stages 13, 16, and 21. Overall, stages with cluster placement in zones with similar Sh_{min} experience comparatively even energy distribution shown in the DAS.

4. Conclusions

Fracture failure models in Evans et al., 2019 suggested that natural fractures within the reservoir open during hydraulic stimulation, so fracture distribution should be considered when determining the placement of perforation clusters. Perforating highly fractured zones within a stage can lead to fracturing fluid preferentially flowing to the cluster or clusters with high natural fracture count rather than expending energy to induce fractures at clusters with few or no natural fractures is that same stage. Stages with all clusters having few or no natural fractures do not have a significantly impact from fracture distribution on the stimulation of that stage. When placing clusters, it is potentially beneficial to avoid sharp peaks in the PR and YME logs that correlate with peaks in bulk density. Those areas are likely the result of increased calcite content which has the potential to "hide" natural, calcite-filled fractures.

Minimum horizontal stress is an effective method of determining cluster placement. Stages with clusters placement in the reservoir with similar Sh_{min} resulted in an even distribution of energy reported in the distributed acoustic sensing data. The calculation of the Sh_{min} magnitudes incorporates several variables which contribute to heterogeneity within the reservoir that can be used when interpreting homogeneous locations to place perforation clusters. Low Sh_{min} did not equal increased energy to a point, so perforating areas of similar Sh_{min} was more effective than perforating the lowest Sh_{min} in an area.

Poisson's Ratio has a close relationship with minimum horizontal stress, and when compared with the DAS data, it was beneficial to keep the PR as constant as possible when placing perforations in the reservoir. Sh_{min} results and the PR results overlap in this analysis, so it would be beneficial to compare the two methods. However, because PR has a comparatively small range in values and because Sh_{min} includes more variables in the calculation, Sh_{min} is a more

effective method of cluster placement when determining homogeneity. Young's Modulus is less effective when determining factors affecting efficient stimulation, though the few examples of significantly higher YME did tie to an increase in strain on the optic fiber at those clusters.

References

Altamar, R.P., and Marfurt, K.J. (2015). Identification of brittle/ductile areas in unconventional reservoirs using seismic and microseismic data: Application to the Barnett Shale: Interpretation, v. 3, p. 233-243.

Anifowoshe, O., M. Yates, L. Xu, P. Dickenson, J. Akin, B. J. Carney, J. Hewitt, I. Costello, and Z. Arnold. (2016). Improving wellbore stimulation coverage in the Marcellus: Integrating lateral measurements with enhanced engineered completion design and fiber optic evaluation: In SPE Eastern Regional Meeting Society of Petroleum Engineers, https://doi.org/10.2118/184051-MS.

Boone, K., Crickmore, R., Werdeg, Z., Laing, C., and Molenaar, M. (2015, July 20). Monitoring Hydraulic Fracturing Operations Using Fiber-Optic Distributed Acoustic Sensing. Unconventional Resources Technology Conference. doi:10.15530/URTEC-2015-2158449

Carr, Timothy R., Wilson, Thomas H., Kavousi, Payam, Amini, Shohreh, Sharma, Shikha, Hewitt, Jay, Costello, Ian, Carney, B.J., Jordon, Emily, Yates, Malcolm, MacPhail, Keith, Uschner, Natalie, Thomas, Mandie, Akin, Si, Magbagbeola, Oluwaseun, Morales, Adrian, Johansen, Asbjoern, Hogarth, Leah, Anifowoshe, Olatunbosun, Naseem, Kashif, Hammack, Richard, Kumar, Abhash, Zorn, Erich, Vagnetti, Robert, and Crandall, Dustin.

(2017). Insights from the Marcellus Shale Energy and Environment Laboratory (MSEEL): Unconventional Resources Technology Conference, DOI: 10.15530-urtec-2017-2670437.

EIA 2020, Annual Energy Outlook 2020: U.S. Energy Information Administration, release date: January 29, 2020, 81p. https://www.eia.gov/outlooks/aeo/.

Engelder T., Lash G.G., Uzcátegui R.S. (2009). Joint sets that enhance production from Middle and Upper Devonian gas shales of the Appalachian Basin. AAPG Bulletin. 93: 857-889. DOI: 10.1306/03230908032

Evans, K., Toth, R., Ore, T., Smith, J., Bannikova, N., Carr, T., and Ghahfarokhi, P. (2019, July 31). Fracture Analysis Before and After Hydraulic Fracturing in the Marcellus Shale Using the Mohr-Coulomb Failure Criteria. Unconventional Resources Technology Conference. doi:10.15530/urtec-2019-650

Ghahfarokhi, Payam K., Carr, Tim, Song, Liaosha, Shukla, Priyavrat, and Pankaj, Piyush. (2018). Seismic Attributes Application for the Distributed Acoustic Sensing Data for the Marcellus Shale: New Insights to Cross-Stage Flow Communication: Society of Petroleum Engineers, SPE-189888.

Ghahfarokhi, P. K., Carr, T., Song, L., Shukla, P., and Pankaj, P. (2018, January 23). Seismic Attributes Application for the Distributed Acoustic Sensing Data for the Marcellus Shale: New Insights to Cross-Stage Flow Communication. Society of Petroleum Engineers. doi:10.2118/189888-MS

Grieser, Bill, and Bray, Jim. (2007). Identification of Production Potential in Unconventional Reservoirs: Society of Petroleum Engineers, SPE-106623.

Grieser, W. V., and Bray, J. M. (2007, January 1). Identification of Production Potential in Unconventional Reservoirs. Society of Petroleum Engineers. doi:10.2118/106623-MS

Jarvie, Daniel M. (2012). Shale Resource Systems for Oil and Gas: Part 1- Shale-gas Resource Systems: American Association of Petroleum Geologists, v. 97, p. 69-87.

King, G.E. (2014). Improving Recovery Factors In Liquids-Rich Resource Plays Requires New Approaches. *Editors Choice Magazine.* Retrieved from http://www.aogr.com/magazine/editors-choice/improving-recovery-factors-in-liquids-rich-resource-plays-requires-new-appr

Kumar, Abhash, Hammack, Richard, and Harbery, William. (2017). Seismic Monitoring of Hydraulic Fracturing Activity at the Marcellus Shale Energy and Environment Laboratory (MSEEL) Site, West Virginia: Unconventional Resources Technology Conference, DOI: 10.15530/urtec-2017-2670481.

Laronga, R. J., and Shalaby, E. (2014, November 1). Borehole Imaging Technology Visualizes Photorealistically in Oil-Based Muds. Society of Petroleum Engineers. doi:10.2118/1114-0036-JPT

MacPhail, W. F. P., Lisoway, B., and Banks, K. (2012, January 1). Fiber Optic Distributed Acoustic Sensing of Multiple Fractures in a Horizontal Well. Society of Petroleum Engineers. doi:10.2118/152422-MS

McConaughy DT, Engelder T. (1999). Joint interaction with embedded concretions: Joint loading configurations inferred from propagation paths. Journal of Structural Geology. 21: 1637-1652. DOI: 10.1016/S0191-8141(99)00106-6

Molenaar, M. M., and Cox, B. E. (2013, January 28). Field Cases of Hydraulic Fracture Stimulation Diagnostics Using Fiber Optic Distributed Acoustic Sensing (DAS) Measurements and Analyses. Society of Petroleum Engineers. doi:10.2118/164030-MS

Molenaar, M. M., Hill, D., Webster, P., Fidan, E., and Birch, B. (2012, March 1). First Downhole Application of Distributed Acoustic Sensing for Hydraulic-Fracturing Monitoring and Diagnostics. Society of Petroleum Engineers. doi:10.2118/140561-PA

Repetski, J.E., Ryder, R.T., Weary, D.J., Harris, A.G., and Trippi, M.H. (2008). Thermal maturity patterns (CAI and %R_o) in Upper Ordovician and Devonian rocks of the Appalachian basin: A major revision of USGS Map I–917–E using new subsurface collections: U.S. Geological Survey Scientific Investigations Map 3006, one CD-ROM.

Song, Liaosha, Paronish, Tom, Agrawal, Vikas, Hupp, Brittany, Sharma, Shikha, and Carr, Timothy. (2017). Depositional Environment and Impact on Pore Structure and Gas Storage Potential of Middle Devonian Organic Rich Shale, Northeastern West Virginia, Appalachian Basin: Unconventional Resources Technology Conference, DOI: 10.1530/urtec-2017-2667397.

U.S. Energy Information Administration - EIA - Independent Statistics and Analysis. (2019, September 5). Retrieved January 16, 2020, from https://www.eia.gov/tools/faqs/faq.php?id=907&t=8

Walker, K. J., Wutherich, K., Terry, J., Shreves, J. E., and Caplan, J. (2012, January 1). Improving Production in the Marcellus Shale Using an Engineered Completion Design: A Case Study. Society of Petroleum Engineers. doi:10.2118/159666-MS

Wang, Guochang, and Carr, Timothy R.. (2013). Organic-rich Marcellus Shale lithofacies modeling and distribution pattern analysis in the Appalachian Basin: American Association of Petroleum Geologists, v. 97, no. 12, p. 2173-2205.

Werne, J.P., B.B. Sageman, T. W. Lyons, and D.J. Hollander. (2002). An integrated assessment of a "type euxinic" deposit: Evidence for multiple controls on black shale deposition in the Middle Devonian Oatka Creek Formation: American Journal of Science, v. 302, p. 110-143, doi: 10.2475/ajs.302.2.110.

Woodrow, D. L., and W. D. Sevon. (1985). The Catskill Delta: Geologic Society of America Special Paper 201, p. 39-49.

Zagorski, W.A., Bowman, Douglas C., Emery, Martin, and Wrightstone, Gregory R.. (2011). An overview of Some Key Factors Controlling Well Productivity in Core Areas of the Appalachian Basin Marcellus Shale Play: American Association of Petroleum Geologists, Article #110147.

Zagorski, William A., Emery, Martin, and Ventura, Jeffrey L. (2017). The Marcellus Shale Play: Its Discovery and Emergence as a Major Global Hydrocarbon Accumulation: American Association of Petroleum Geologists, v. 113, p. 55-90.

Zagorski, W. A., Emery, M., and Ventura, J. L. (2017). The Marcellus Shale Play: Its Discovery and Emergence as a Major Global Hydrocarbon Accumulation. *American Association of Petroleum Geologists, Memoir (113)*, 55-90. doi:10.1306/13572001M1133491

Zamirian, M., Aminian, K., and Ameri, S. (2016, May 23). Measuring Marcellus Shale Petrophysical Properties. Society of Petroleum Engineers. doi:10.2118/180366-MS

Zhu, Y., and Carr, T. R. (2018, October 5). Estimation of Fracability of the Marcellus Shale: A Case Study from the MIP3H in Monongalia County, West Virginia, USA. Society of Petroleum Engineers. doi:10.2118/191818-18ERM-MS

Zhu, Yixuan, Petrophysical and Geomechanical Characterization of the Marcellus Shale in the Appalachian Basin, unpublished PhD dissertation, West Virginia University, 85p.

Zoback, M. D. and Kohli, A. H. (2019). *Unconventional Reservoir Geomechanics: Shale gas, Tight Oil, and Induced Seismicity*. United Kingdom: Cambridge University Press.

Zoback, M. D. (2014). *Reservoir Geomechanics*. United Kingdom: Cambridge University Press.

Zorn, Erich, Harbert, William, Hammack, Richard, and Kumar, Abhash. (2017). Geomechanics Of the Microseismic Response to Devonian Organic Shales at the Marcellus Shale Energy and Environment (MSEEL) Site, West Virginia: Unconventional Resources Technology Conference, DOI: 10.15530/urtec-2017-2669946.